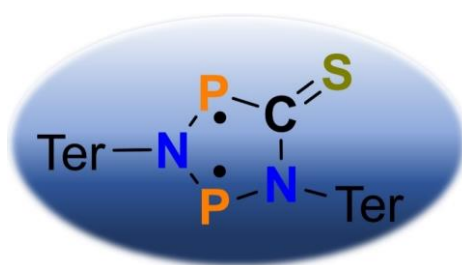


SUPPORTING INFORMATION

A Cyclic Thioketone as Biradical Heterocyclopentane-1,3-diyl: Synthesis, Structure and Activation Chemistry

Henrik Beer,^[a] Alexander Linke,^[a,b] Jonas Bresien,^[a] Alexander Villinger, and Axel Schulz,^{[a,b]*}



This file includes:

1	Experimental	2
2	Structure elucidation.....	4
3	Syntheses of compounds	13
4	Additional spectroscopic data	41
5	Computational details	49
6	References.....	52

1 Experimental

General information. If not stated otherwise, all manipulations were carried out under oxygen- and moisture-free conditions in an inert argon atmosphere using standard Schlenk or drybox techniques. All glassware was heated three times *in vacuo* using a heat gun and cooled under argon atmosphere. Solvents were transferred using syringes, which were purged three times with argon prior to use. Solvents and reactants were either obtained from commercial sources or synthesized as detailed in Table S1.

Table S1: Origin and purification of solvents and reactants.

Substance	Origin	Purification
THF	Fisher Scientific, 99.5%	dried over Na/benzophenone freshly distilled prior to use
<i>n</i> -hexane, C ₆ H ₆ , toluene	local trade	dried over Na/benzophenone/tetraglyme freshly distilled prior to use
C ₆ D ₆	euriso-top	dried over Na freshly distilled prior to use
THF- <i>d</i> ₈	euriso-top	dried over Na distilled and stored over molecular sieves (4 Å)
Mg-turnings	abcr, 99.8%, for Grignards	can be activated by stirring for several weeks under argon using a glass coated magnetic stir bar.
thiophosgene	old stock	freshly distilled
CS ₂	Riedel-de Haën	dried over P ₄ O ₁₀ , freshly distilled prior to use
benzaldehyde	Sigma Aldrich	freshly distilled
KOtBu	old stock	sublimed
[P(μ -NTer)] ₂	synthesized ¹	re-crystallized as described in the literature

NMR spectra were recorded on Bruker spectrometers (AVANCE 250, AVANCE 300 or AVANCE 500) and were referenced internally to the deuterated solvent (C₆D₆ δ_{ref} = 128.4 ppm), to protic impurities in the deuterated solvent (C₆HD₅ δ_{ref} = 7.16 ppm,

THF-*d*₇ $\delta_{\text{ref},1} = 1.73$ ppm, $\delta_{\text{ref},2} = 3.58$ ppm) or externally (³¹P: 85% H₃PO₄ $\delta_{\text{ref}} = 0$ ppm). All measurements were carried out at ambient temperature unless denoted otherwise.

IR spectra of crystalline samples were recorded on a Bruker Alpha II FT-IR spectrometer equipped with an ATR unit at ambient temperature under argon atmosphere. Relative intensities are reported according to the following intervals: very weak (vw, 0–10%), weak (w, 10–30%), medium (m, 30–60%), strong (s, 60–90%), very strong (vs, 90–100%).

Raman spectra of crystalline samples were recorded using a LabRAM HR 800 Horiba Jobin YVON Raman spectrometer equipped with an Olympus BX41 microscope with variable lenses. The samples were excited by a red laser (633 nm, 17 mW, air-cooled HeNe laser). All measurements were carried out at ambient temperature unless stated otherwise.

Elemental analyses were obtained using an Elementar vario Micro cube CHNS analyser.

Melting points (uncorrected) were determined using a Stanford Research Systems EZ Melt at a heating rate of 20 °C/min. Clearing points are reported.

Mass spectra were recorded on a Thermo Electron MAT 95-XP sector field mass spectrometer using crystalline samples or an Advion Expression L benchtop mass spectrometer (*m/z* 10–2000) equipped with an Advion Expression CMS detector using sample solutions or crystalline samples.

UV-Vis spectra were acquired on a Perkin-Elmer Lambda 19 UV-Vis spectrometer or an Agilent Cary 60 UV-vis spectrometer using 6Q quartz cuvettes (*d* = 10 mm).

2 Structure elucidation

X-ray structure determination: X-ray quality crystals were selected in Fomblin YR-1800 perfluoroether (Alfa Aesar) at ambient temperature. The samples were cooled to 123(2) K during measurement. The data were collected on a Bruker D8 Quest diffractometer or a Bruker Kappa Apex II diffractometer using Mo K α radiation ($\lambda = 0.71073$ Å). The structures were solved by iterative methods (SHELXT)² and refined by full matrix least squares procedures (SHELXL).³ Semi-empirical absorption corrections were applied (SADABS).⁴ All non-hydrogen atoms were refined anisotropically, hydrogen atoms were included in the refinement at calculated positions using a riding model.

Table S2: Crystallographic details.

Compound	$[\text{P}(\mu\text{-N}^{\text{Ter}})]_2(\text{CS})\cdot\text{CS}_2$	$\{[\text{SP}(\mu\text{-N}^{\text{Ter}})\text{PS}]\text{TerNCCSMg}\}_2$	$[\text{P}(\mu\text{-N}^{\text{Ter}})]_2(\text{CS})\cdot\text{CS}_2$ tempered
Chem. Formula	$0.965 \text{ C}_{50}\text{H}_{50}\text{N}_2\text{P}_2\text{S}_3 \cdot$ $0.035 \text{ C}_{49}\text{H}_{50}\text{N}_2\text{P}_2\text{S}_2 \cdot$ $0.5 \text{ C}_6\text{H}_{14}$	$\text{C}_{100}\text{H}_{100}\text{Mg}_2\text{N}_4\text{P}_4\text{S}_6 \cdot$ $2 \text{ C}_6\text{H}_6$	$\text{C}_{75}\text{H}_{75}\text{N}_3\text{P}_2\text{S}_3 \cdot$ $1.75 \text{ C}_6\text{H}_{14}$
Formula weight [g/mol]	878.25	1878.91	1327.30
Colour	green	yellow	yellow
Crystal system	monoclinic	monoclinic	triclinic
Space group	$P2_1/n$	$P2_1/c$	$P\bar{1}$
a [Å]	11.3291(4)	14.7772(8)	13.6583(11)
b [Å]	33.4090(12)	26.1230(13)	16.3349(13)
c [Å]	12.5659(5)	26.2318(11)	19.1061(15)
α [°]	90	90	71.092(2)
β [°]	95.810(1)	97.283(2)	81.928(3)
γ [°]	90	90	68.473(2)
V [Å ³]	4731.7(3)	10044.4(9)	3750.3(5)
Z	4	4	2
$\rho_{\text{calcd.}}$ [g/cm ³]	1.233	1.242	1.175
μ [mm ⁻¹]	0.26	0.26	0.19
T [K]	123(2)	123(2)	173(2)
Measured reflections	165506	291304	200415
Independent reflections	13782	24260	17233
Reflections with $I > 2\sigma(I)$	10507	14324	13217
R_{int}	0.062	0.138	0.064
$F(000)$	1864	3968	1423
$R_1(R[F^2 > 2\sigma(F^2)])$	0.041	0.057	0.045
$wR_2(F^2)$	0.106	0.145	0.112
GooF	1.03	1.06	1.07
No. of Parameters	579	1263	766
CCDC #	2153624	2153626	2153625

Compound	[P(μ -NTer)] ₂ (CS)·PhCHO	[P(μ -NTer)] ₂ (CSCl ₂) ^[a]
Chem. Formula	C ₅₆ H ₅₆ N ₂ OP ₂ S	C ₄₉ H ₅₀ Cl ₂ N ₂ P ₂ S
Formula weight [g/mol]	867.02	831.81
Colour	yellow	yellow
Crystal system	orthorhombic	orthorhombic
Space group	<i>P</i> 2 ₁ 2 ₁ 2 ₁	<i>P</i> 2 ₁ 2 ₁ 2 ₁
<i>a</i> [Å]	12.033(3)	11.8588(8)
<i>b</i> [Å]	15.815(4)	17.0939(13)
<i>c</i> [Å]	24.673(5)	21.7897(16)
α [°]	90	90
β [°]	90	90
γ [°]	90	90
<i>V</i> [Å ³]	4695.3(18)	4417.1(6)
<i>Z</i>	4	4
$\rho_{\text{calcd.}}$ [g/cm ³]	1.227	1.251
μ [mm ⁻¹]	0.18	0.30
<i>T</i> [K]	123(2)	123(2)
Measured reflections	221057	62960
Independent reflections	15631	7346
Reflections with <i>I</i> > 2 σ (<i>I</i>)	13549	6262
<i>R</i> _{int}	0.058	0.125
<i>F</i> (000)	1840	1752
<i>R</i> ₁ (<i>R</i> [<i>F</i> ² > 2 σ (<i>F</i> ²)])	0.037	0.146
<i>wR</i> ₂ (<i>F</i> ²)	0.097	0.319
GooF	1.05	1.17
No. of Parameters	572	599
CCDC #	2153623	–[a]

[a] As the crystals were very small and intergrown due to 3 different isomers, the data quality is rather poor, and the structure solution only serves as proof of connectivity. Therefore no CCDC number was requested.

2.1 $[P(\mu\text{-N}^t\text{er})]_2(\text{CSCl}_2)$

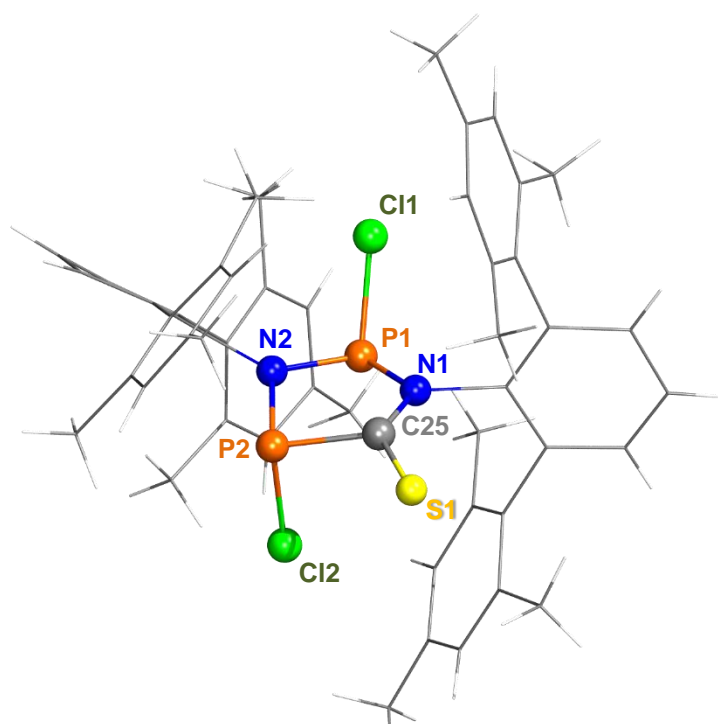


Figure S1: Ball-and-stick representation of the molecular structure of **7** in the crystal. Only a ball-and-stick representation is shown due to a poor data set.

2.2 $[\text{P}(\mu\text{-N}^{\text{Ter}})]_2(\text{CS})\cdot\text{CS}_2$ (layer A 96.5%)

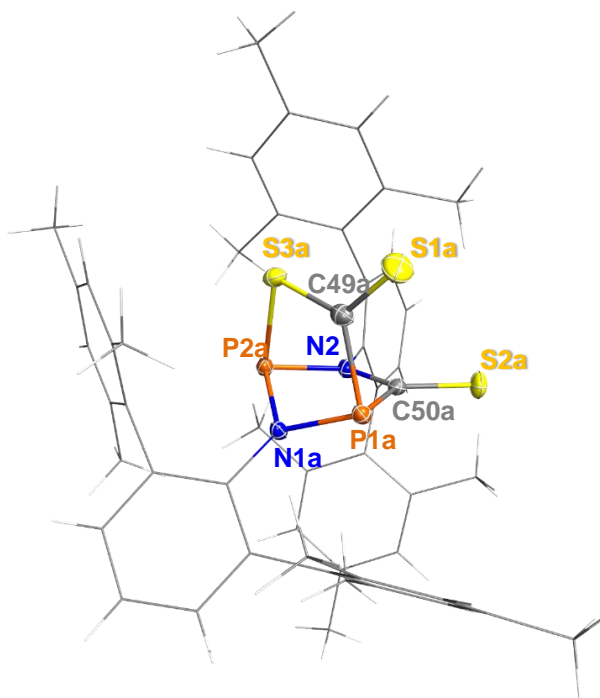


Figure S2: ORTEP of **9** in the crystal. Ellipsoids set at 50% probability (123 K).

2.3 $[\text{P}(\mu\text{-N}^t\text{er})]_2(\text{CS})\cdot\text{CS}_2$ (layer B 3.5%)

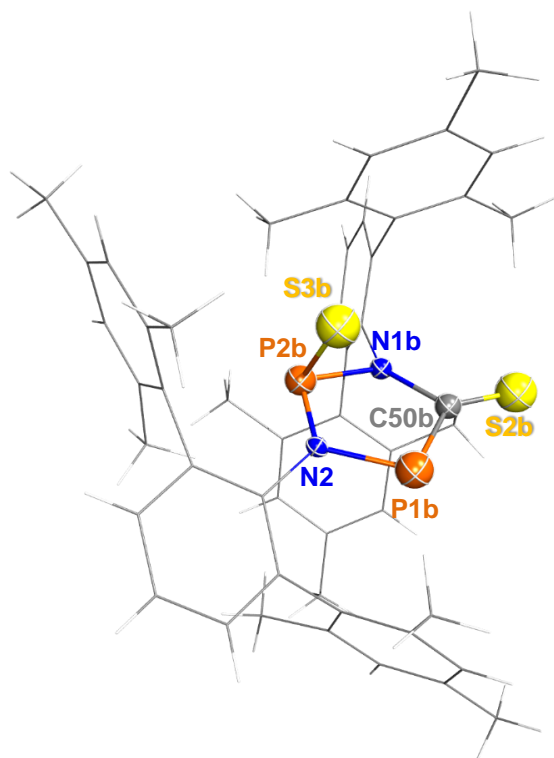


Figure S3: ORTEP of **10** (Layer B of compound **9**) in the crystal. Ellipsoids set at 50% probability (123 K).

2.4 $\{[\text{SP}(\mu\text{-N}^{\text{Ter}})\text{PS}]\text{TerNCCSMg}\}_2$

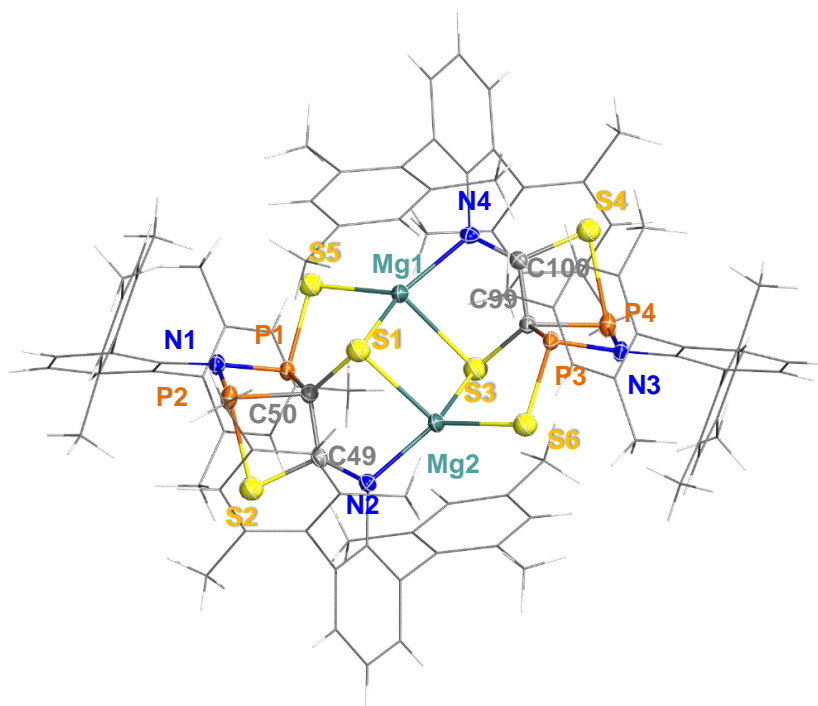


Figure S4: ORTEP of **8** in the crystal. Ellipsoids set at 50% probability (123 K).

2.5 $[\text{P}(\mu\text{-N}^t\text{er})]_2(\text{CS})\cdot\text{CS}_2$

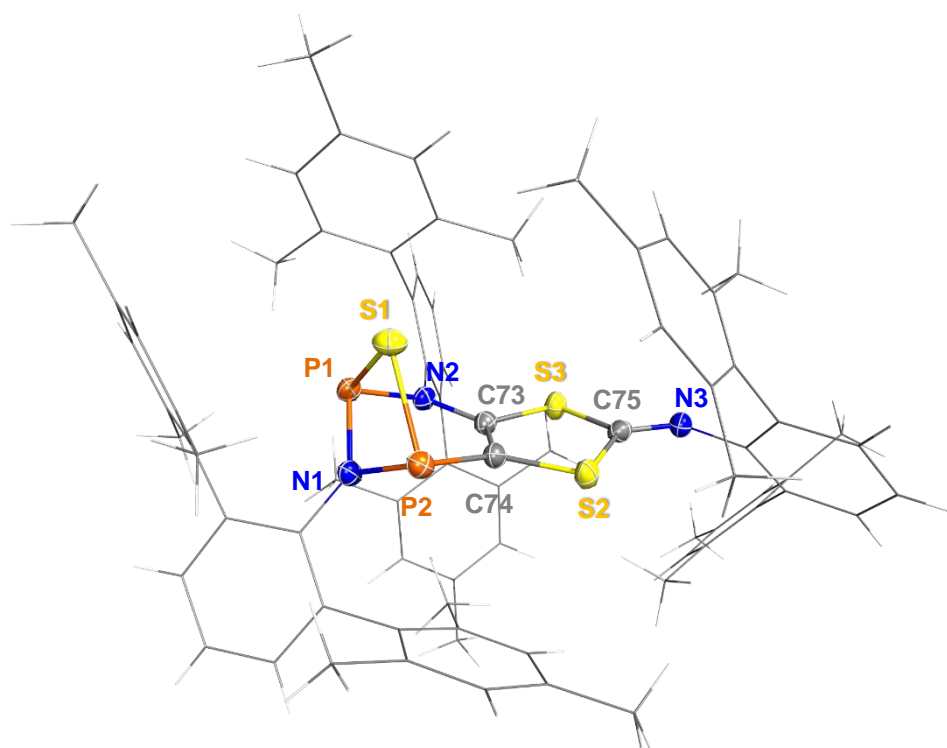


Figure S5: ORTEP of **13** in the crystal. Ellipsoids set at 50% probability (173 K)

2.6 $[P(\mu\text{-N}^t\text{er})]_2(\text{CS})\cdot\text{PhCHO}$

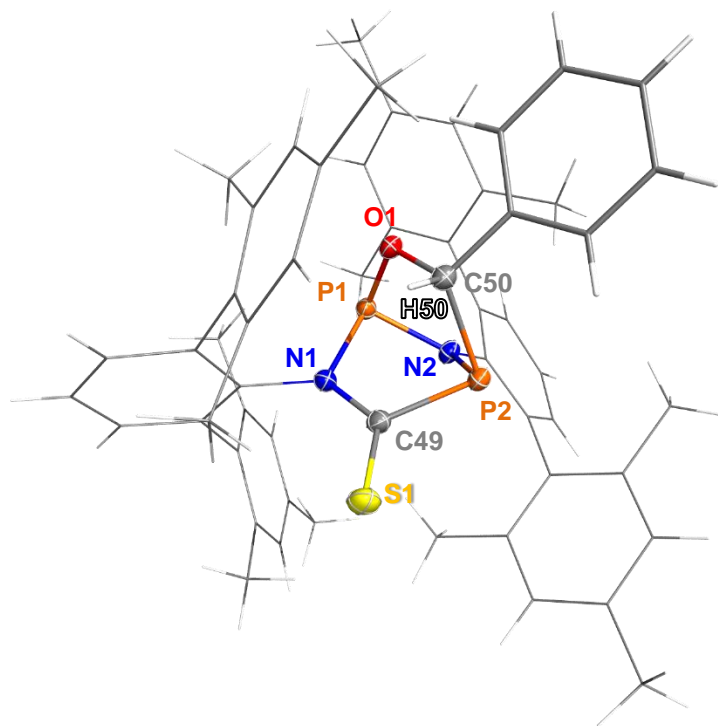
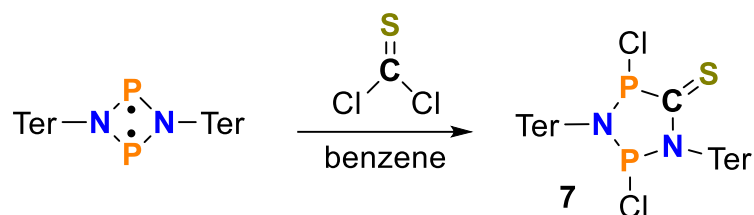


Figure S6: ORTEP of **14** in the crystal. Ellipsoids set at 50% probability (123 K).

3 Syntheses of compounds

3.1 $[P(\mu\text{-N}Ter)]_2(CSCl_2)$ – Compound 7



$[P(\mu\text{-N}Ter)]_2$ (1.20 g, 1.67 mmol) was dissolved in benzene (15 mL). The solution was cooled to 7 °C (cold water with ice) and thiophosgene (192 mg, 1.67 mmol) was added dropwise. An immediate colour change from red to yellow was observed. After stirring for one hour at ambient temperature, all volatile components were removed *in vacuo* (1×10^{-3} mbar) and the yellow residue was dried *in vacuo* (1×10^{-3} mbar) for 30 min at 50 °C (water bath). The residue was re-dissolved in benzene (4 mL) and the product was crystallized from a minimal amount of fresh benzene at ambient temperature. The supernatant was removed by syringe and the crystals were dried *in vacuo* (1×10^{-3} mbar) for 30 minutes at 40 °C (water bath). Yield: 973 mg (1.17 mmol, 70%).

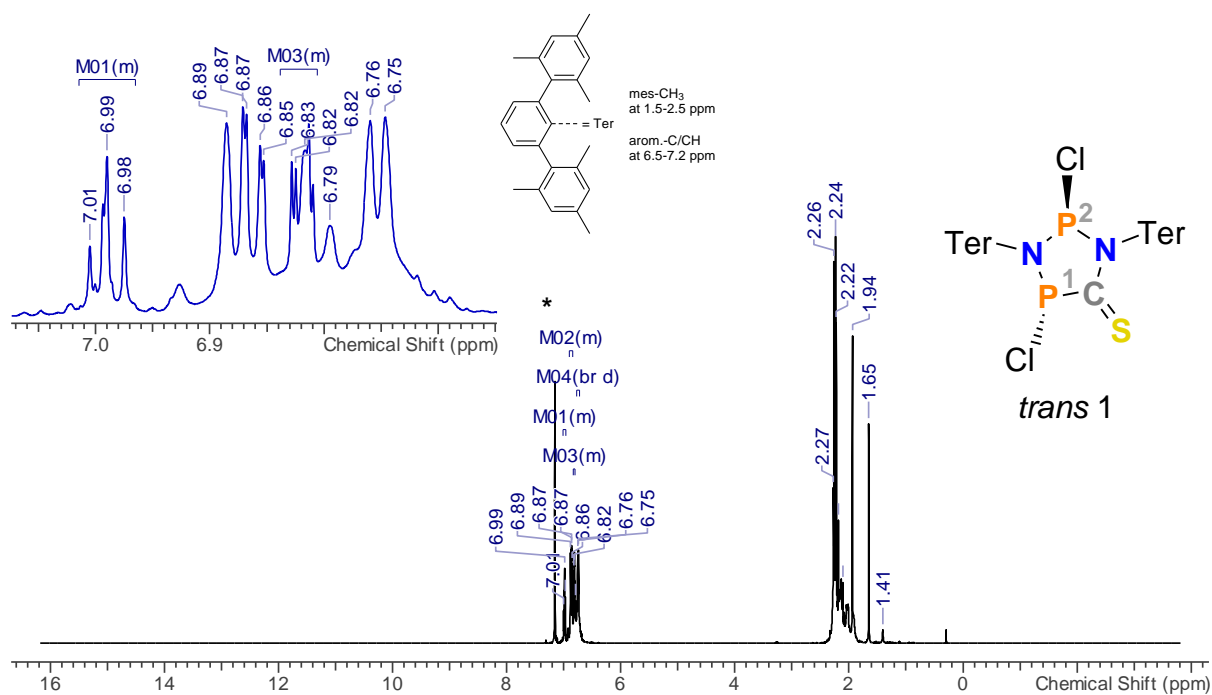
Due to the presence of an isomeric mixture the quality of the crystals was only sufficient for a structural proof.

C₄₉H₅₀N₂P₂Cl₂S (831.86 g/mol). **Mp.** 180 °C – 189 °C (decomp.). **CHN** calc. (found) in %: C 70.75 (70.84), H 6.06 (6.56), N 3.37 (3.21), S 3.85 (4.73). In solution, 3 different isomers can be observed (*trans*1/ *trans*2/ *cis* (10 : 60 : 1)). **¹H NMR** (25 °C, C₆D₆, 500.1 MHz): δ = 1.65 (s, CH₃), 1.94 (s, CH₃), 2.19 (s, CH₃), 2.22 (s, CH₃), 2.24 (s, CH₃), 2.26 (s, CH₃), 6.66–7.02 (m, CH). **³¹P{¹H} NMR** (25 °C, C₆D₆, 205.5 MHz): δ = 96.6 (s, *cis*), 98.3 (s, *trans* 2), 100.2 (s, *trans* 1), 162.1 (s, *cis*), 175.2 (s, *trans* 2), 195.4 (s, *trans* 1). **¹³C{¹H} NMR** (25 °C, C₆D₆, 125.8 MHz): δ = 21.4 (s, CH₃), 21.5 (s, CH₃), 22.5 (s, CH₃),

22.8 (s, CH₃), 23.0 (s, CH₃), 125.5 (s, arom. C), 126.7 (s, arom. C), 129.1 (s, arom. C), 129.3 (s, arom. C), 129.4 (s, arom. C), 129.6 (s, arom. C), 129.7 (s, arom. C), 130.5 (s, arom. C), 131.0 (s, arom. C), 131.3 (s, arom. C), 132.6 (s, arom. C), 132.7 (s, arom. C), 135.5 (s, arom. C), 136.1 (s, arom. C), 136.6 (s, arom. C), 136.9 (s, arom. C), 137.1 (s, arom. C), 137.2 (s, arom. C), 137.4 (s, arom. C), 137.6 (s, arom. C), 137.8 (s, arom. C), 138.2 (s, arom. C), 139.3 (s, arom. C), 142.6 (d, $^1J(^{13}\text{C}, ^{31}\text{P}) = 1.4 \text{ Hz}$, CS), 142.9 (d, $^1J(^{13}\text{C}, ^{31}\text{P}) = 1.8 \text{ Hz}$, CS). **¹⁴N NMR** (25 °C, C₆D₆, 18.1 MHz): No signals observed. **¹⁵N HMBC NMR** (25 °C, C₆D₆, 50.7 MHz): No signals observed. **Raman** (633 nm, 10 s, 10 scans, cm⁻¹): $\tilde{\nu} = 3153$ (1), 3048 (2), 3009 (2), 2917 (4), 2856 (1), 2731 (1), 1612 (4), 1578 (3), 1482 (1), 1433 (2), 1403 (2), 1380 (3), 1303 (8), 1281 (2), 1268 (2), 1242 (1), 1227 (1), 1193 (3), 1189 (3), 1159 (1), 1099 (4), 1087 (2), 1052 (2), 1004 (1), 991 (1), 944 (1), 909 (1), 897 (1), 847 (1), 810 (1), 738 (2), 722 (01), 661 (1), 652 (1), 641 (1), 606 (1), 593 (1), 574 (7), 554 (4), 525 (2), 509 (2), 501 (2), 491 (3), 481 (2), 424 (10), 405 (2), 386 (1), 335 (2), 317 (1), 297 (1), 280 (2), 265 (2), 248 (4), 225 (3). **IR** (ATR, 25 °C, 32 Scans, cm⁻¹): $\tilde{\nu} = 2996$ (w), 2949 (w), 2912 (m), 2854 (w), 2730 (w), 2324 (vw), 1945 (vw), 1881 (vw), 1721 (vw), 1628 (w), 1611 (m), 1576 (w), 1484 (w), 1447 (m), 1403 (m), 1377 (m), 1298 (w), 1265 (s), 1179 (s), 1162 (m), 1096 (w), 1084 (m), 1051 (w), 1030 (m), 1008 (w), 909 (s), 903 (s), 896 (s), 880 (s), 847 (s), 810 (m), 800 (s), 773 (m), 752 (m), 738 (m), 694 (m), 661 (m), 635 (w), 606 (w), 593 (m), 575 (w), 567 (w), 556 (w), 536 (m), 492 (vs), 480 (s), 439 (s), 424 (s), 412 (s). **MS** (CI pos., *iso*-butane) *m/z* (%): 330 [Ter-NH₃]⁺, 340, 358, 396, 456, 679, 751 [C₄₈H₅₀ClN₂P₂]⁺, 786 [C₄₈H₅₀Cl₂N₂P₂]⁺, 831 [M⁺ + H⁺].

Figure S7: NMR, IR and Raman spectra of $[P(\mu\text{-Nter})]_2(\text{CSCl}_2)$ (solvent signals indicated by asterisks).

^1H NMR spectrum, C_6D_6 , 500.1 MHz



$^{31}\text{P}\{^1\text{H}\}$ NMR spectrum, C_6D_6 , 205.5 MHz, *P1* at lower numbers

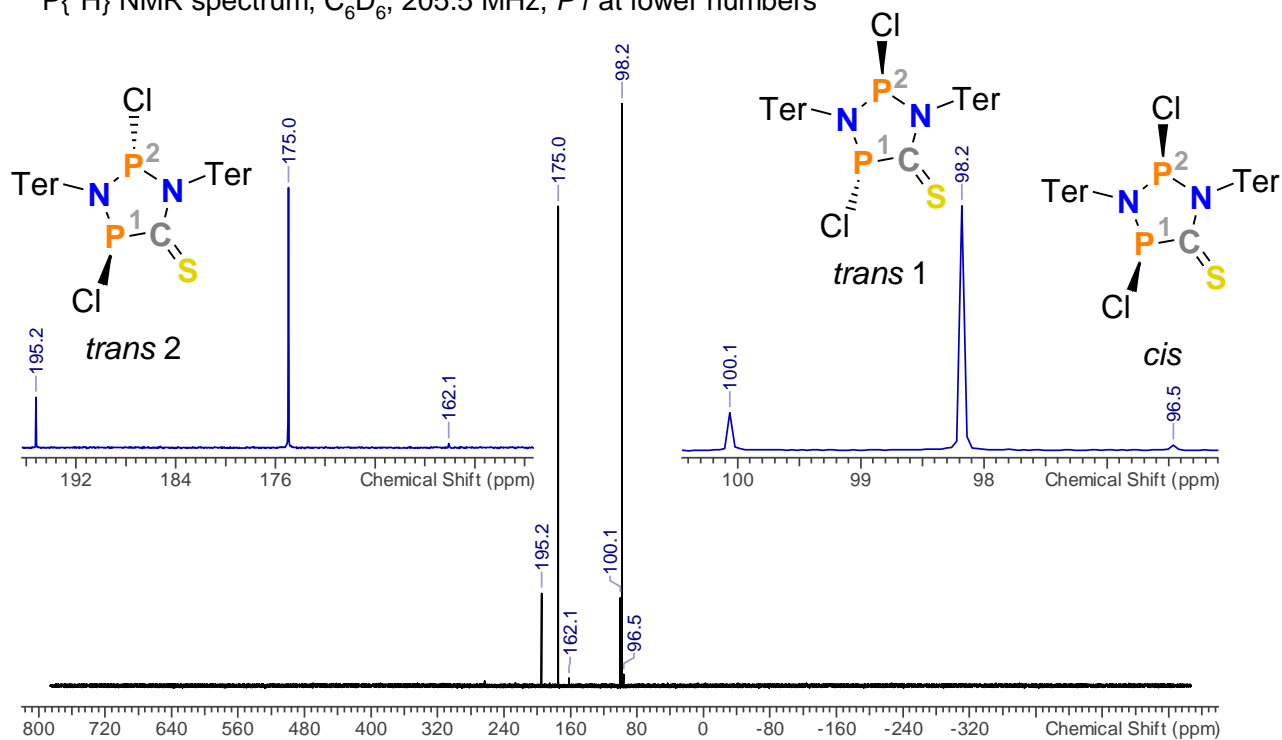
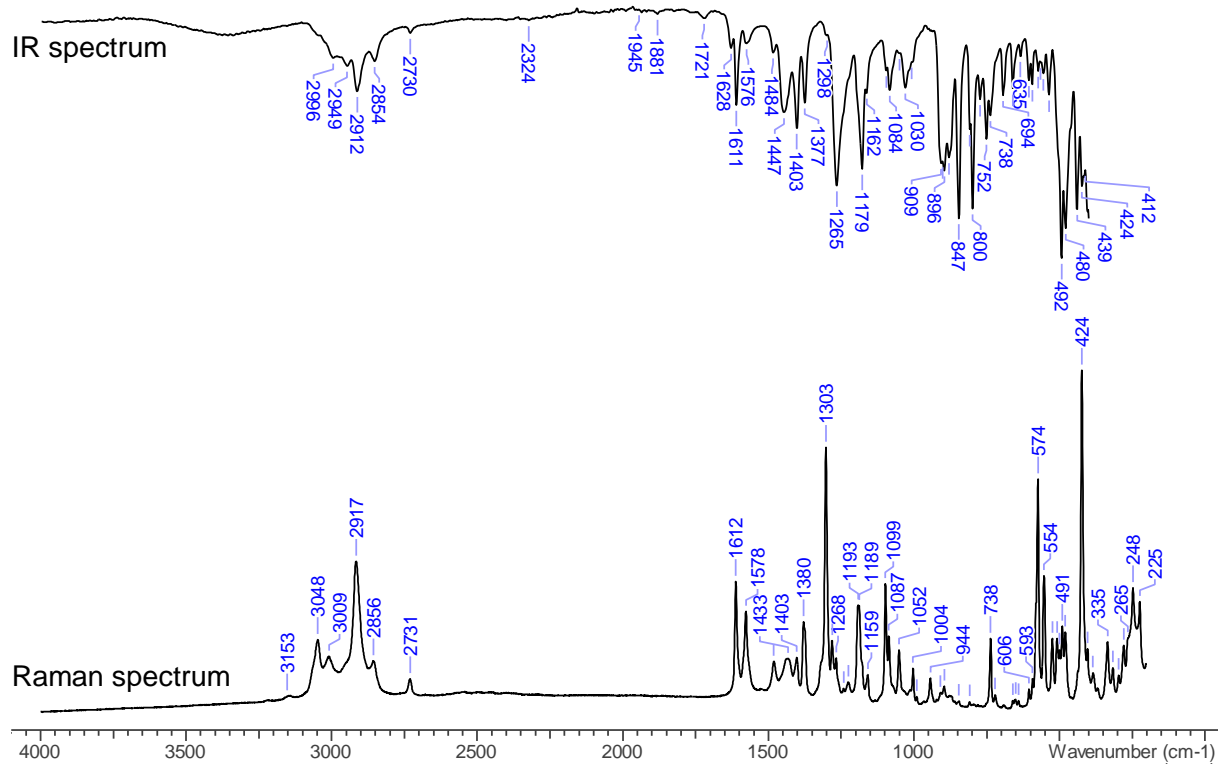
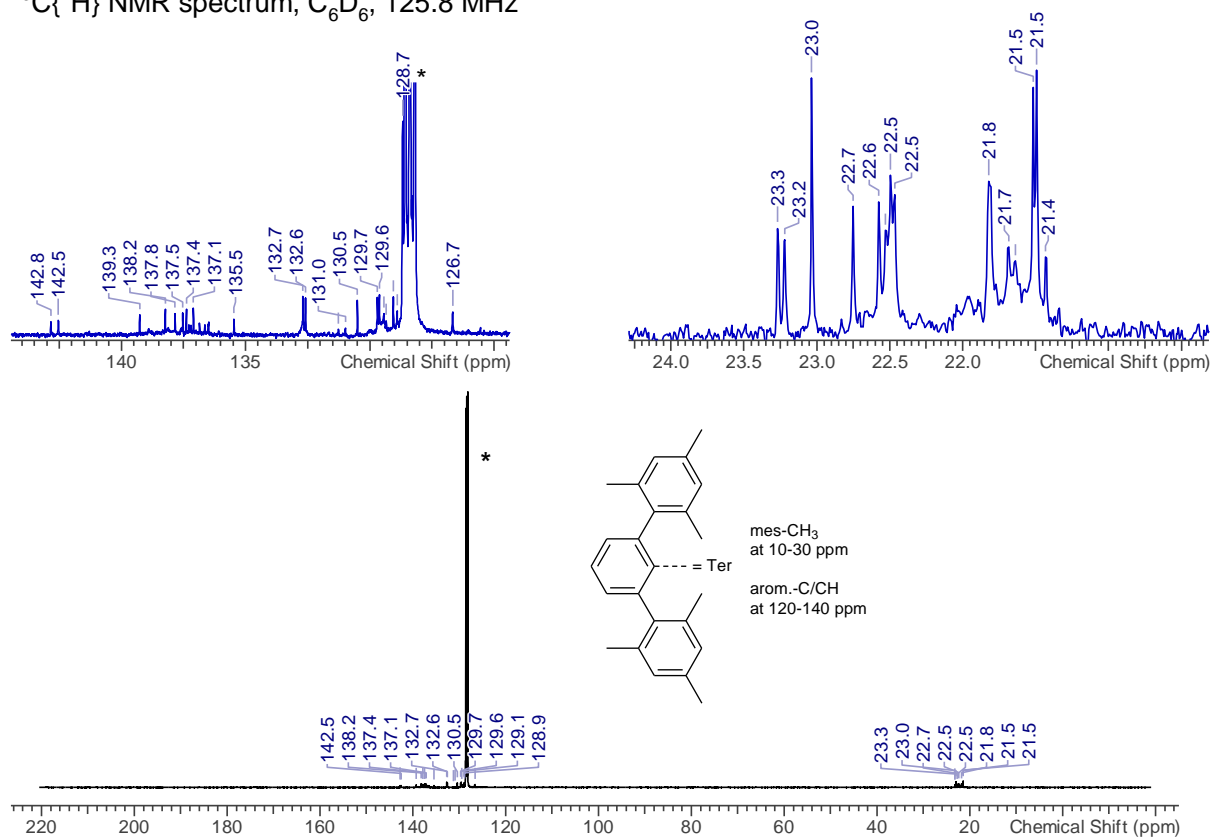
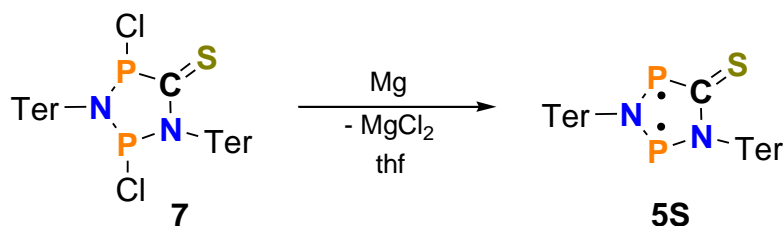


Figure S7. continued.

$^{13}\text{C}\{^1\text{H}\}$ NMR spectrum, C_6D_6 , 125.8 MHz



3.2 Synthesis of $[P(\mu\text{-N}^{\bullet}\text{Ter})]_2(\text{CS})$ – Biradical **5S**



$[P(\mu\text{-N}^{\bullet}\text{Ter})]_2(\text{CSCl}_2)$ (500 mg, 0.60 mmol) and Mg turnings (43.7 mg, 10.2 mmol) were combined in a Schlenk flask. *Attention: It is paramount to ensure that no grease finds its way into the reaction vessel.* THF (10 mL) was added and the reaction mixture was stirred at ambient temperature. The pale yellow mixture gradually turned green and finally deep blue. *The progress of the reaction was monitored by $^{31}\text{P}\{^1\text{H}\}$ NMR spectroscopy, as over-reduction and decomposition occurred quickly.* When the reaction was nearly completed, the solution was separated from magnesium, the solvent was removed *in vacuo* (1×10^{-3} mbar), and the solid residue was dried at 40 °C (water bath) for 30 minutes. Benzene (15 mL) was added, and the insoluble material was separated by filtration. If necessary, the cloudy filtrate was filtered a second time over a celite-packed frit. All volatile components were removed *in vacuo* (1×10^{-3} mbar) and intensively blue residue was dried *in vacuo* (1×10^{-3} mbar) for 30 min at 50 °C (water bath). Yield: 0.408 g (0.540 mmol, 90%).

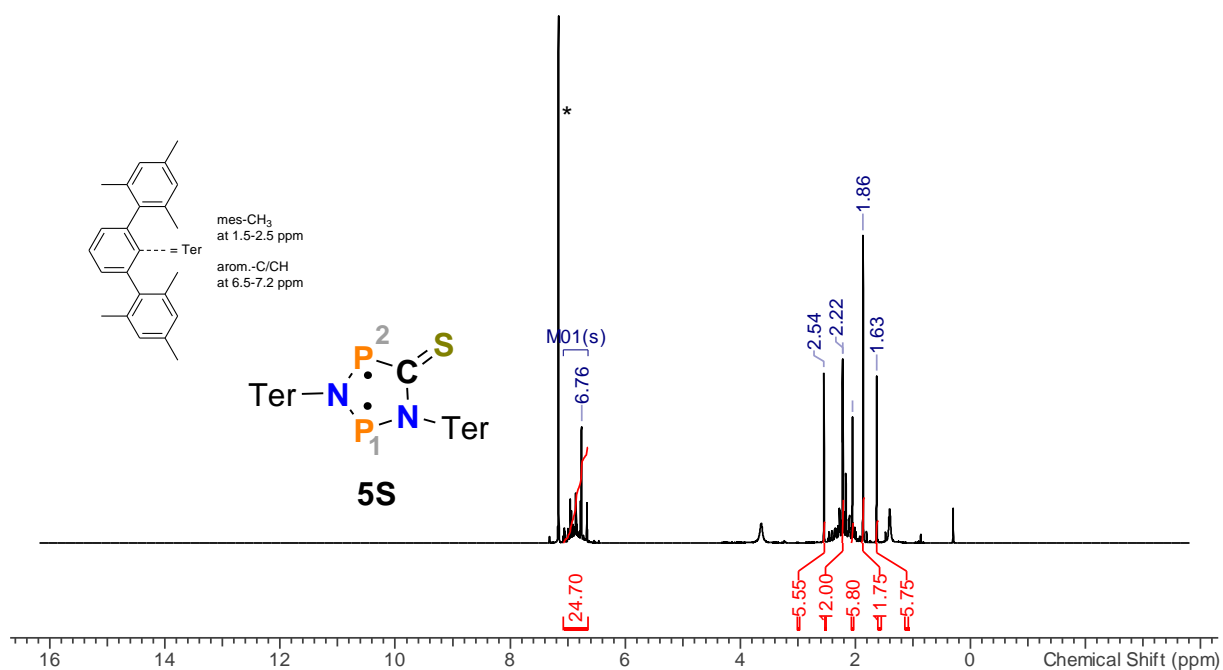
The product is stable as a solid at –20 °C in the darkness for a short period.

Note: When exposed to light, the product **5S** decomposes very rapidly under elimination of Ter-NC and other (mostly unidentified) products. All work must be carried out under exclusion of light from the time of reduction. A freshly prepared solution of **5S** has a purity of ca. 90% (observed by-products: $[P(\mu\text{-N}^{\bullet}\text{Ter})]_2(\text{CSCl}_2)$ (**7**), $[\text{CIP}(\mu\text{-N}^{\bullet}\text{Ter})]_2$, TerNC, $[\text{TerNPNTer}]\text{MgCl}\cdot\text{THF}$ and further undefinable impurities). However, despite great care, these by-products always occur and clean isolation/crystallization was not possible. Furthermore, the amount of decomposition products increases rapidly with time (and depending on the temperatures, light etc.), which means that work must always be done quickly and in the dark.

C₄₉H₅₀N₂P₂S (760.96 g/mol). **Mp.** Mixture: 125 °C (decomp.). **CHN** calc. (found) in %: C 77.34 (66.26), H 6.62 (6.10), N 3.68 (2.79), S 4.21 (3.21). The deviation of the elemental analysis results from the difficulties of synthesis (light, humidity, air, see section 3.2). **¹H NMR** (25 °C, C₆D₆ and THF, 500.1 MHz): δ = 1.63 (s), 1.86 (s), 2.05 (s), 2.16 (s), 2.21 (s), 2.22 (s), 2.54 (s), 6.67-7.08 (m). **³¹P{¹H} NMR** (25 °C, C₆D₆ and THF, 205.5 MHz): δ = 81.4 (s), 100.2 (s, (compound **7**)), 157.3 (s), 195.4 (s, (compound **7**)), 243.0 (d, 1P, $^2J(^1\text{H}, ^{31}\text{P}) = 87$ Hz, CPN), 226.5 (s, ([CIP(μ -NTer)]₂), 263.4 (s, ([CIP(μ -NTer)]₂), 289.5 (d, 1P, $^2J(^1\text{H}, ^{31}\text{P}) = 87$ Hz, NPN). **Raman:** Due to decomposition under light, it was not possible to analyze the product by Raman spectroscopy. **IR** (ATR, 25 °C, 32 Scans, cm⁻¹): $\tilde{\nu}$ = 3349 (m), 2969 (m), 2947 (m), 2916 (m), 2854 (m), 2728 (w), 2116 (w), 1632 (m), 1611 (m), 1574 (w), 1484 (w), 1442 (m), 1407 (m), 1374 (m), 1269 (m), 1259 (m), 1220 (m), 1191 (m), 1164 (m), 1115 (m), 1088 (m), 1067 (m), 1030 (s), 971 (m), 911 (m), 882 (s), 847 (vs), 802 (s), 775 (m), 748 (s), 738 (s), 688 (s), 645 (s), 600 (s), 573 (s), 558 (s), 542 (s), 538 (s), 525 (s), 511 (s), 495 (vs), 482 (s), 470 (s), 441 (vs), 408 (vs). **MS** (ESI pos., THF) m/z (%): 330 [Ter-NH₃]⁺, 761 [M⁺ + H⁺], 831 [[P(μ -NTer)]₂(CSCl₂)]⁺. **UV-Vis** (benzene, 0.0013 mol/L): $\lambda_{\text{max.}}$ = 638 nm (0.67)

Figure S8. NMR, IR and UV-Vis spectra of $[\text{P}(\mu\text{-Nter})]_2(\text{CS})$ (solvent signals indicated by asterisks).

^1H NMR spectrum, C_6D_6 and THF, 500.1 MHz



$^{31}\text{P}\{^1\text{H}\}$ NMR spectrum, C_6D_6 THF, 205.5 MHz

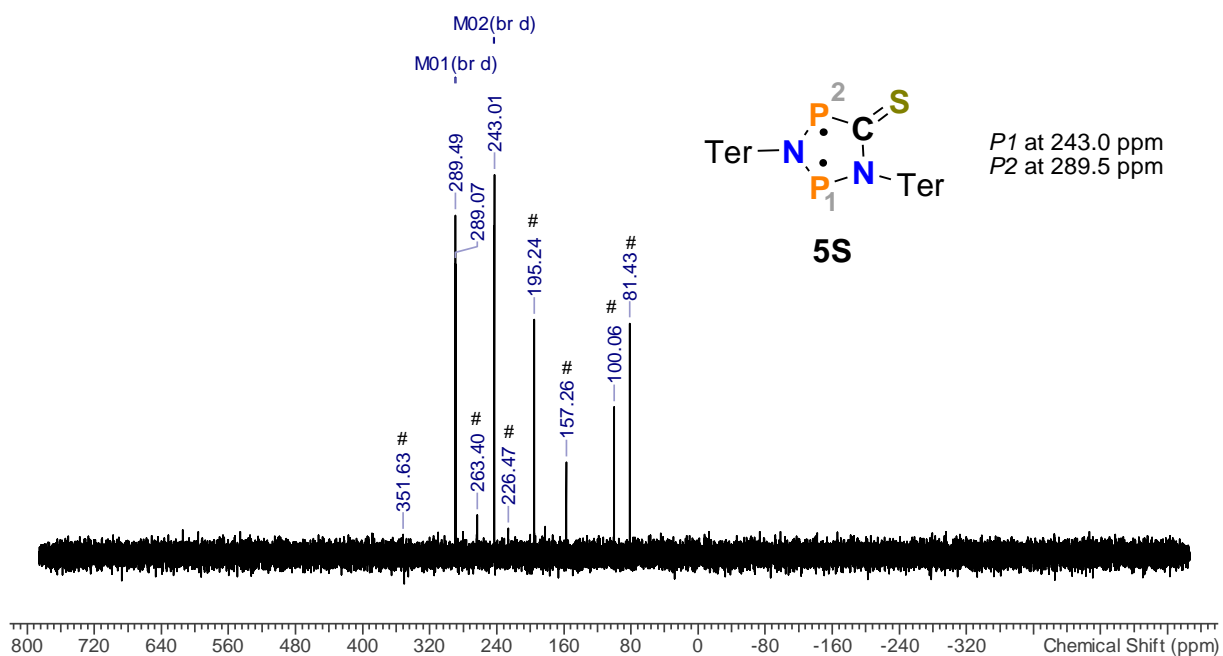
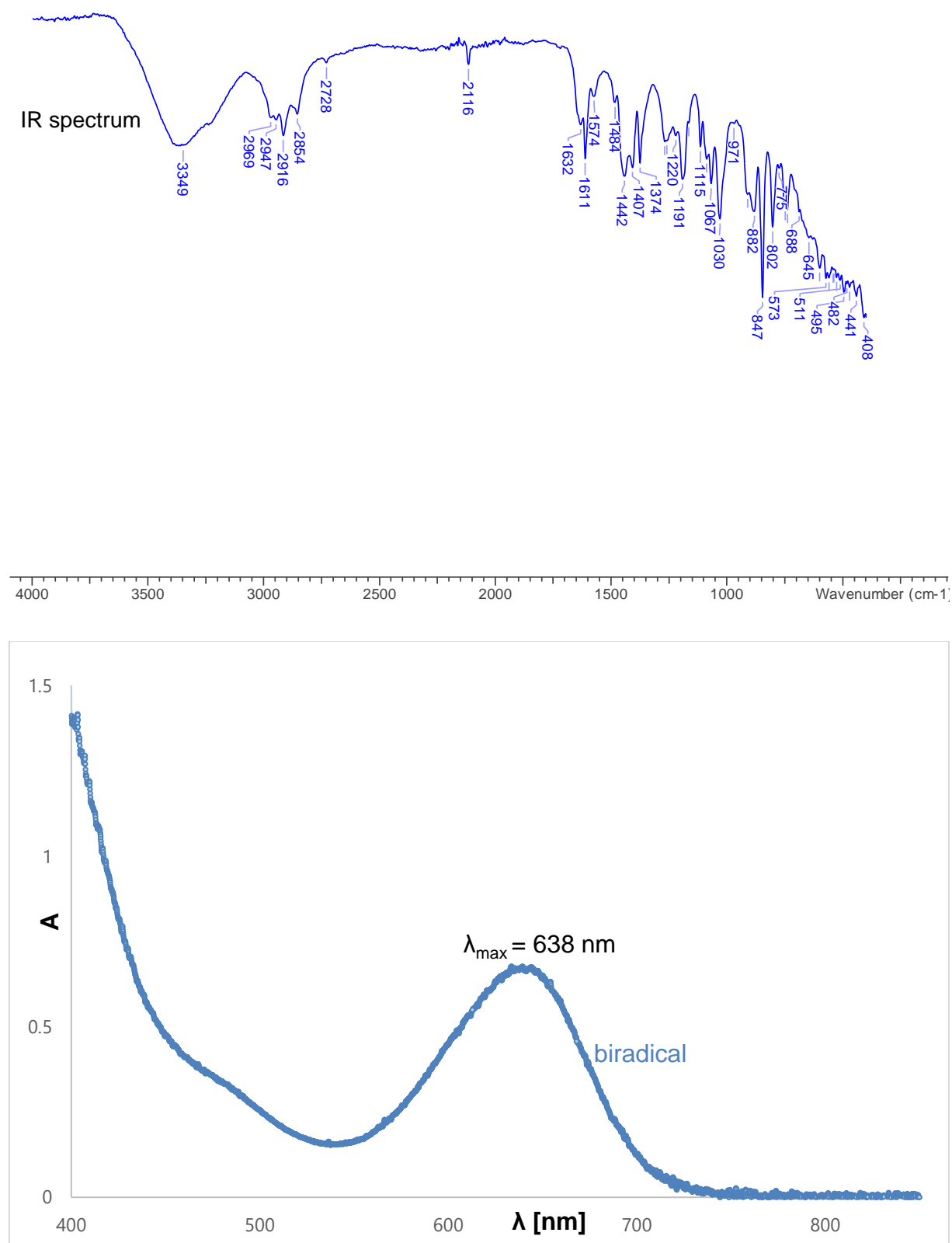
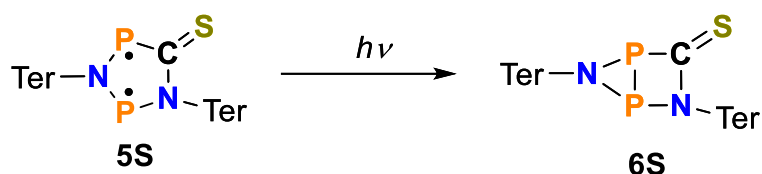


Figure S8. continued.



3.3 Generation of the housane-type species $[P(\mu\text{-N}^{\text{Ter}})]_2(\text{CS})$ (**6S**)



The housane **6S** could be generated by irradiation of a freshly prepared solution of blue biradical **5S** (638 nm, 500 mA, $-20\text{ }^{\circ}\text{C}$) with red light ($\lambda_{\text{max.}} = 638\text{ nm}$).

Note: Due to the very strong light sensitivity of the biradical **5S**, the product can only be observed *in-situ* in the $^{31}\text{P}\{^1\text{H}\}$ NMR spectrum and therefore could not be analyzed further. As soon as the biradical **5S** is irradiated with light to produce the housane **6S**, the decomposition reaction of **6S** to undefined products begins. Moreover, a freshly prepared solution of **5S** has a purity of ca. 90% (see chapter 3.2).

^1H NMR Due to the broadness of the THF signals, evaluation of the ^1H NMR is not possible. Figure S9 shows the ^1H NMR spectrum. **$^{31}\text{P}\{^1\text{H}\}$ NMR** (253 K, THF- d_8 , 101.3 MHz): $\delta = -81.5$ (d, 1P, $^1J(^{31}\text{P}, ^{31}\text{P}) = 22\text{ Hz}$), -101.0 (d, 1P, $^1J(^{31}\text{P}, ^{31}\text{P}) = 22\text{ Hz}$).

Figure S9. NMR and UV-Vis spectra of of the housane-type species of $[P(\mu\text{-N}Ter)]_2(\text{CS})$ (solvent signals indicated by asterisks).

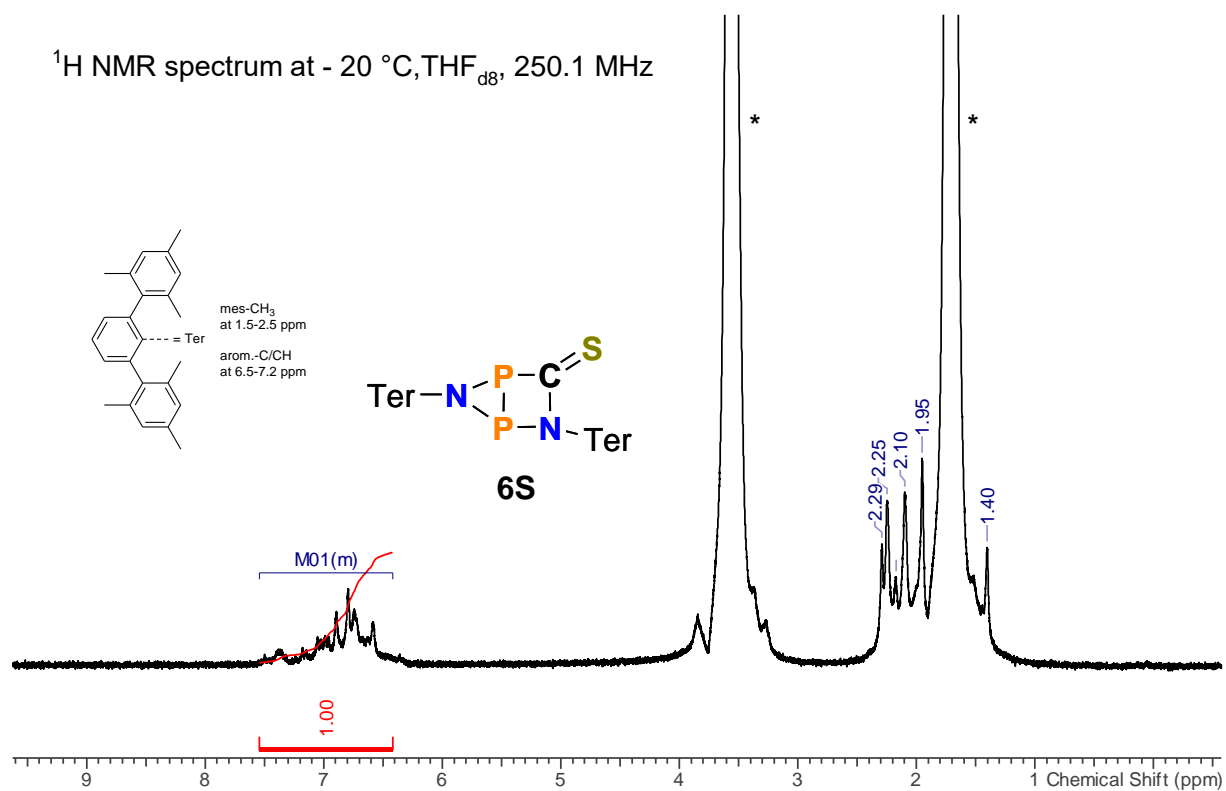
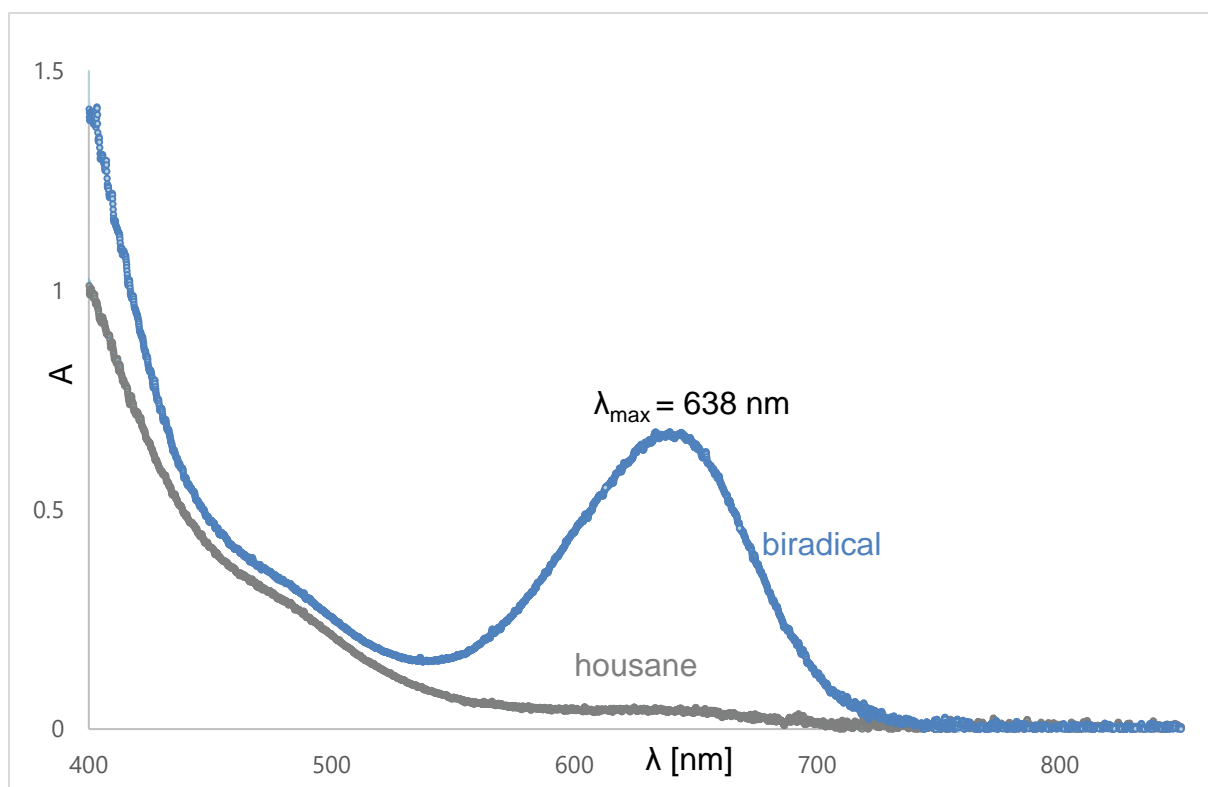
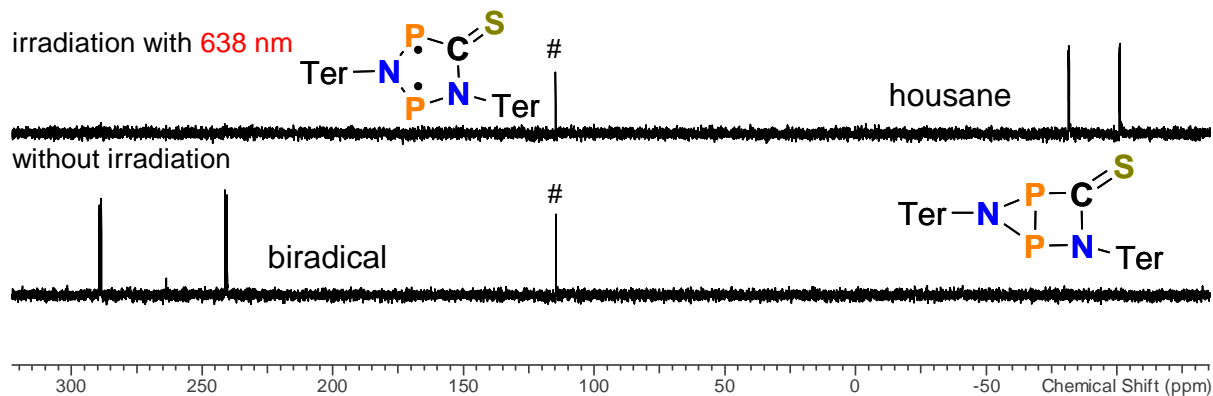
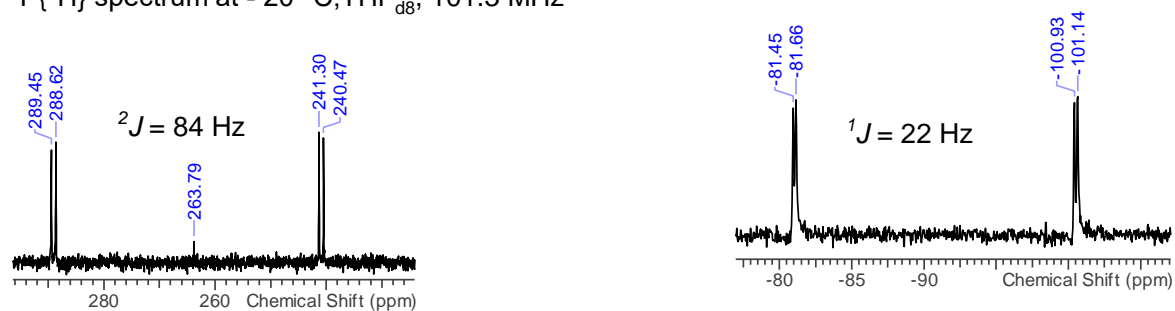
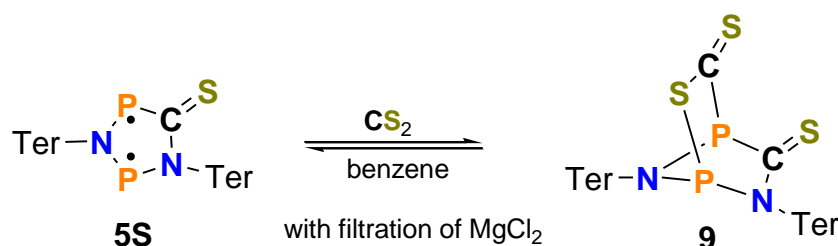


Figure S9. continued.

$^{31}\text{P}\{^1\text{H}\}$ spectrum at $-20\text{ }^\circ\text{C}$, $\text{THF}_{\text{d}8}$, 101.3 MHz



3.4 Reaction of Biradical **5S** with CS₂ with filtration of MgCl₂ – Synthesis of [P(μ -N $\overline{\text{Ter}}$)]₂(CS)·CS₂ (**9**)



Note: Due to the very strong light sensitivity of the biradical **5S**, it should be prepared freshly and *in situ*. As soon as the biradical **5S** is irradiated with light, decomposition reactions begin. Such a freshly prepared solution of **5S** has a purity of ca. 90% (see chapter 3.2).

All experiments were attempted as best as possible under complete exclusion of light to avoid decomposition of the biradical.

[P(μ -N $\overline{\text{Ter}}$)]₂(CS) (200 mg, 0.26 mmol) was dissolved in benzene (10 mL) and CS₂ (20 mg, 16 μ L, 0.26 mmol) was added dropwise. An immediate colour change from deep blue to green was observed. After stirring for 10 minutes at ambient temperature, all volatile components were removed *in vacuo* (1×10^{-3} mbar) and the green residue was dried *in vacuo* (1×10^{-3} mbar) for 30 min at ambient temperature. The residue was re-dissolved in *n*-hexane (50 mL) and the flask was connected to another flask *via* a Schlenk frit. The system was degassed by several freeze-pump-thaw cycles. The insoluble material of the saturated suspension was removed by filtration. After concentration of the filtrate at ambient temperature, the solution was stored at 5 °C overnight, resulting in the deposition of green crystals. The supernatant was removed by syringe and the crystals were dried *in vacuo* (1×10^{-3} mbar) for 30 minutes at ambient temperature. Yield: 80 mg raw product (0.09 mmol, 35%).

Single crystals suitable for X-ray diffraction can be grown from saturated *n*-hexane solution at 5 °C.

*Despite all care and repeated recrystallization, it was impossible to isolate the pure compound without by-products. Both the by-products during the reduction ([TerNPNTer]MgCl*THF and [P(μ-NTer)]₂(CSCl₂) **7**,) and subsequent reaction of the bridged species **9** with the light-induced decomposition product (e.g. MgCl₂ section 3.5 and TerNC section 3.6) could not be separated. The following analytical data are therefore only from the contaminated product.*

C₅₀H₅₀N₂P₂S₃ (878.25 g/mol). **Mp.** 110 °C (decomp.). **CHN** calc. (found) in %: C 71.74 (71.47), H 6.02 (5.82), N 3.35 (2.94), S 11.49 (4.87). The deviation of the elemental analysis results from the difficulties of synthesis (light, humidity, air, see section 3.2). **¹H NMR** (25 °C, C₆D₆, 300.1 MHz): δ = 1.59 (s), 1.81 (s), 2.03 (s), 2.08 (s), 2.10 (s), 2.17 (s), 2.21 (s), 2.23 (s), 2.26 (s), 2.32 (s), 6.65–7.04 (m). **³¹P{¹H} NMR** (25 °C, C₆D₆, 121.5 MHz): δ = 88.4 (d, 1P, ²J(¹H,³¹P) = 16 Hz, CPN), 177.2 (d, 1P, ²J(¹H,³¹P) = 16 Hz, NPN). **¹³C{¹H} NMR** (25 °C, C₆D₆, 125.8 MHz): δ = 19.9 (s), 20.8 (s), 20.8 (s), 20.9 (s), 21.0 (s), 21.1 (s), 21.2 (s), 21.3 (s), 21.5 (s), 22.0 (s), 22.2 (s), 22.3 (s), 124.0 (s), 128.0 (s), 128.4 (s), 128.5 (s), 128.6 (s), 128.7 (s), 128.7 (s), 128.9 (s), 129.0 (s), 129.5 (s), 130.1 (s), 131.3 (s), 131.5 (s), 132.3 (s), 135.3 (s), 135.4 (s), 136.0 (s), 136.1 (s), 136.3 (s), 136.6 (s), 136.7 (s), 136.7 (s), 137.2 (s), 137.4 (s), 137.5 (s), 137.7 (s), 137.9 (s), 138.2 (s), 139.5 (s), 139.6 (s), 140.9 (s), 141.7 (s), 174.7 (s), 192.3 (s, CS₂). **¹⁴N NMR** (25 °C, C₆D₆, 18.1 MHz): No signals observed. **¹⁵N HMBC NMR** (25 °C, C₆D₆, 50.7 MHz): No signals observed. **Raman** (633 nm, 5 s, 5 scans, cm⁻¹): $\tilde{\nu}$ = 3073 (2), 3050 (2), 3009 (2), 2919 (8), 2880 (3), 2877 (3), 2859 (3), 2732 (1), 1613 (2), 1581 (7), 1520 (1), 1484 (2), 1434 (4), 1415 (6), 1380 (3), 1306 (9), 1282 (4), 1273 (4), 1253 (6), 1188 (2), 1162 (1), 1094 (5), 1017 (1), 1007 (2), 949 (2), 740 (2), 657 (2), 650 (1), 605 (1), 594 (6), 581 (10), 562 (5), 525 (5), 513 (6), 492 (3), 488 (4), 477 (3), 453 (1), 435 (1), 423 (1), 410 (2), 383 (1), 353 (2), 337 (2), 329 (2), 304 (2), 276 (3), 261 (4), 246 (4), 243 (4), 234 (4), 189 (3), 172 (4), 161 (4), 151 (3), 148 (3). **IR** (ATR, 25 °C, 32 Scans, cm⁻¹): $\tilde{\nu}$ = 2965 (w), 2943 (m), 2914 (m), 2854 (m), 2730 (w), 2050

(vw), 2038 (vw), 1611 (m), 1576 (w), 1492 (w), 1436 (s), 1409 (s), 1374 (m), 1263 (m), 1222 (m), 1185 (m), 1082 (m), 1067 (m), 1030 (m), 1014 (m), 944 (m), 913 (m), 892 (m), 880 (m), 847 (vs), 812 (s), 797 (s), 787 (s), 760 (vs), 740 (s), 694 (s), 651 (m), 608 (m), 596 (m), 575 (m), 556 (m), 542 (m), 532 (m), 515 (m), 495 (s), 482 (m), 472 (m), 464 (m), 443 (s), 420 (s), 412 (s). **MS** (ESI pos., THF) m/z (%): 330 [Ter-NH₃]⁺, 687, 716 [[P(μ -NTer)]₂]⁺, 831 [[P(μ -NTer)]₂(CSCl₂)]⁺, 879 [M⁺ + H⁺].

Figure S10. NMR, IR and Raman spectra of [P(μ -NTer)]₂(CS)-CS₂ (solvent signals indicated by asterisks).

¹H NMR spectrum, C₆D₆, 300.1 MHz

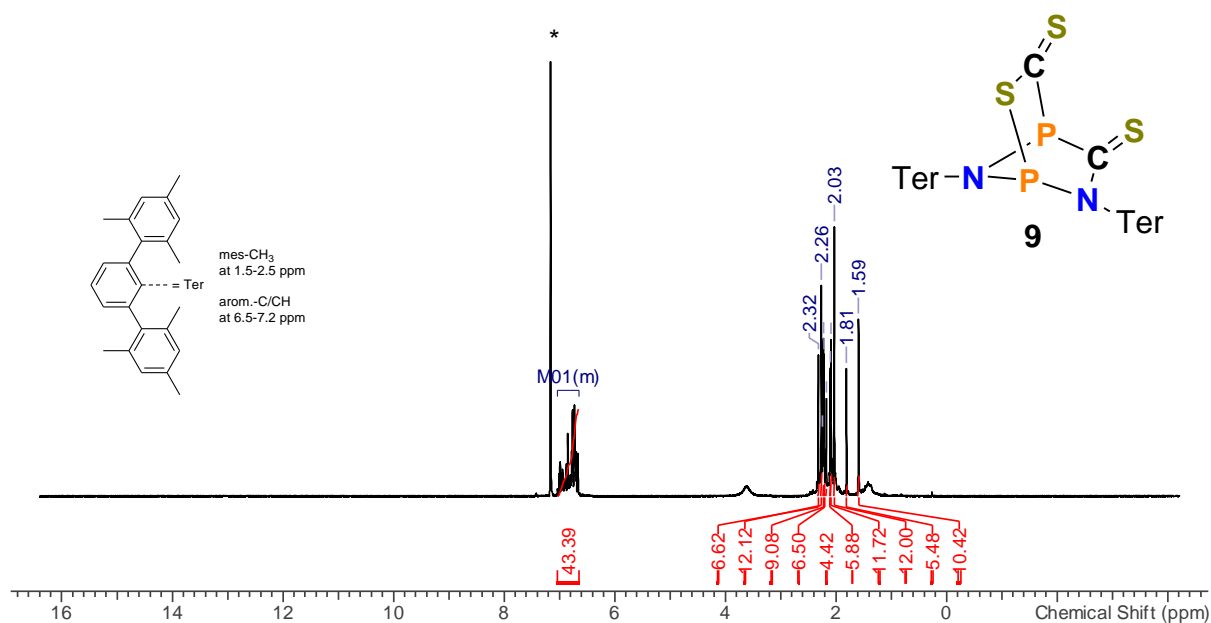


Figure S10. continued.

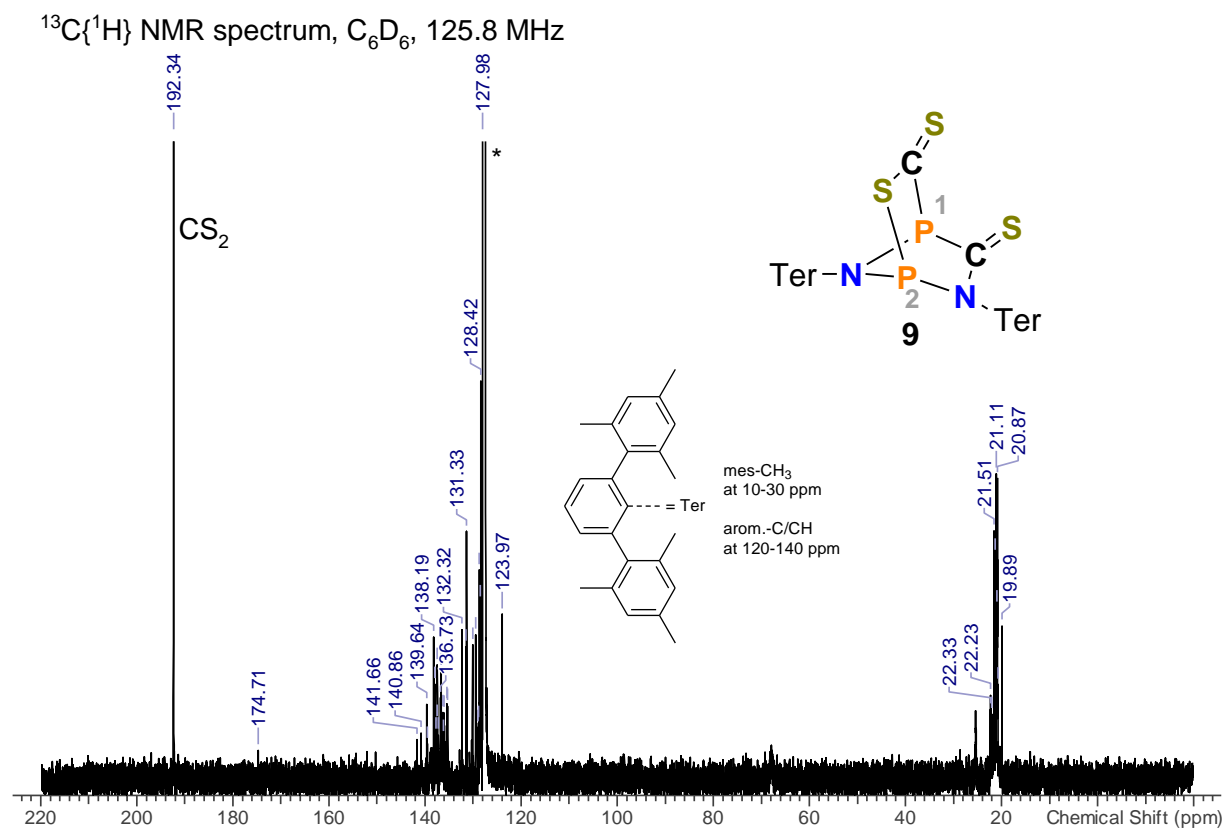
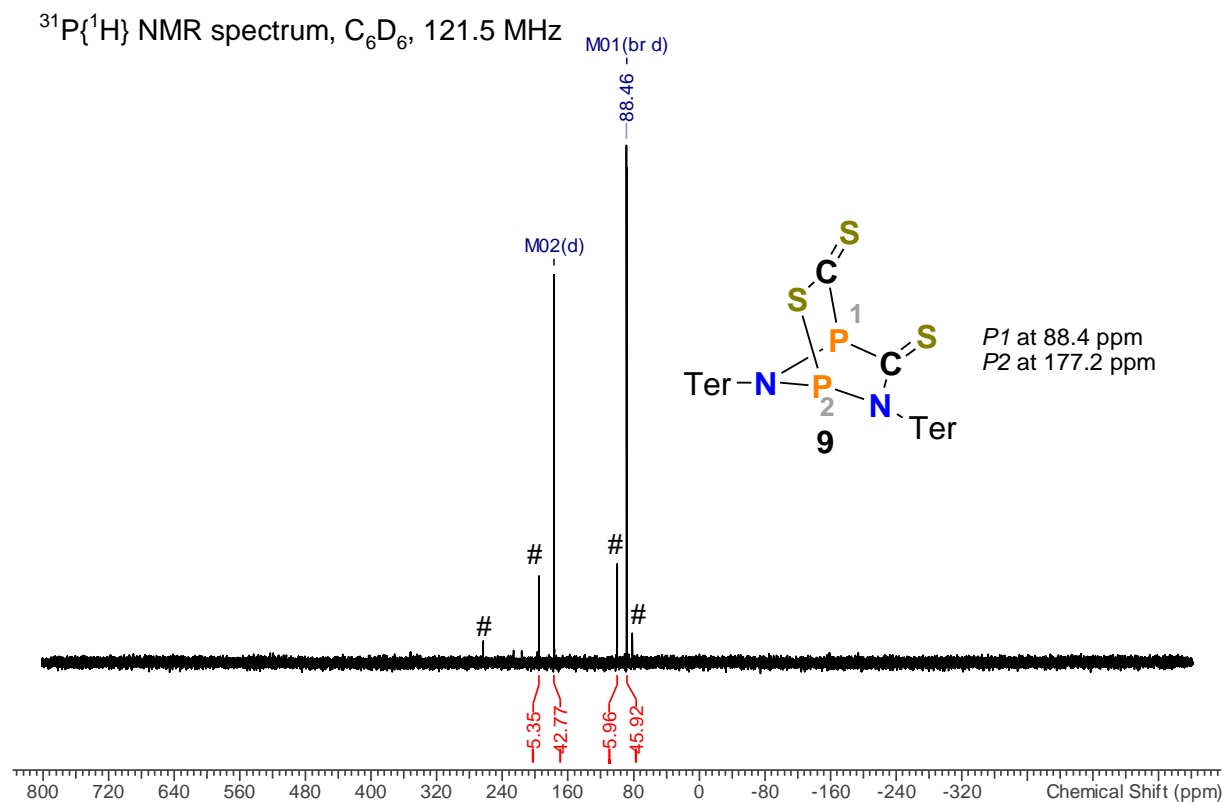
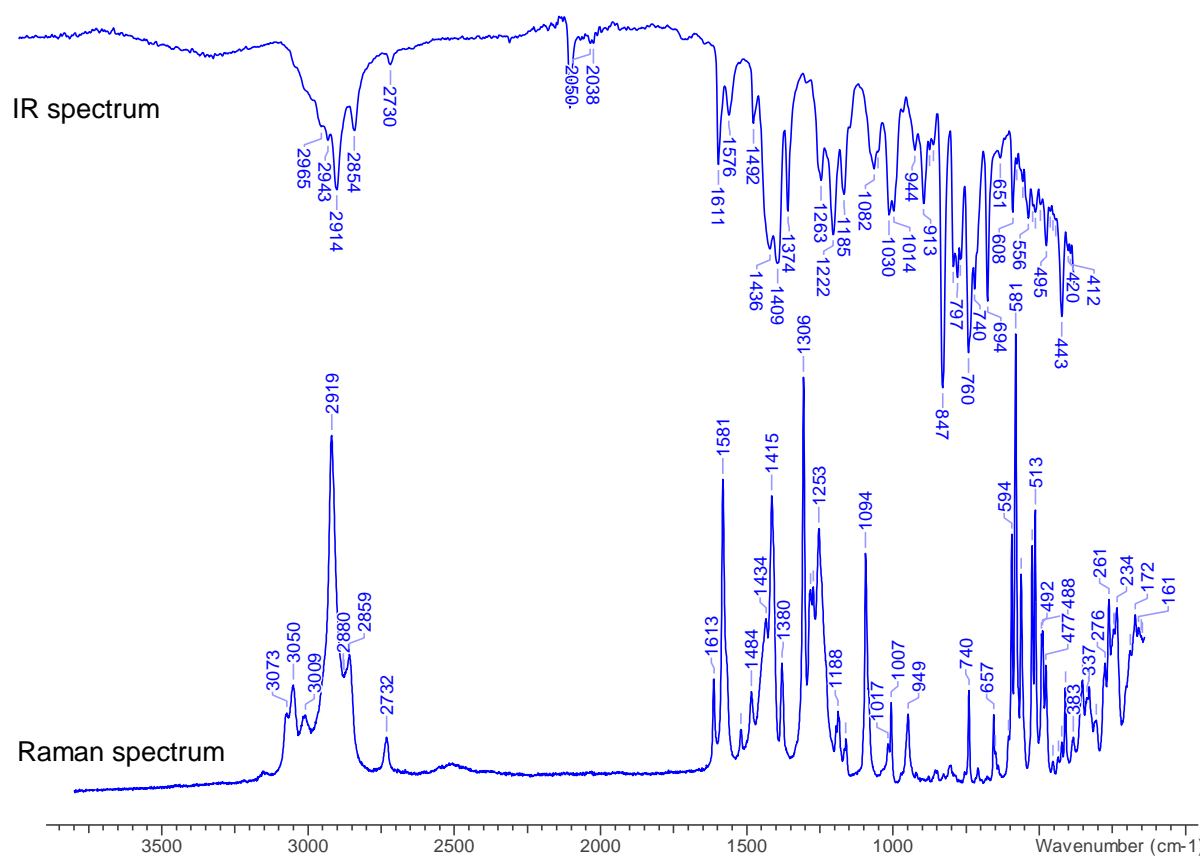
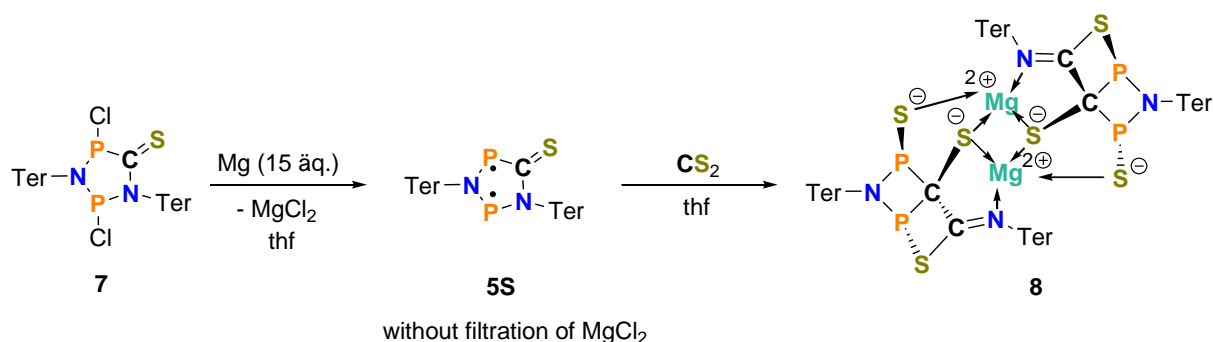


Figure S10. continued.



3.5 Reaction of 5S with CS₂ without filtration – Synthesis of magnesium salt 8: {[SP(μ-NTer)PS]TerNCCSMg}₂



[P(μ-NTer)]₂(CSCl₂) (100 mg, 0.12 mmol) and Mg were combined in a vial and THF (3 mL) was added. The golden yellow solution was stirred vigorously using a glass covered stir bar. After about 10 minutes, the solution turned green and then deep blue. *The progress of the reaction was monitored by ³¹P{¹H} NMR spectroscopy, as over-reduction and decomposition occurred quickly.* When most of the starting material was reduced (decomposition products could already be observed in ³¹P NMR spectrum), CS₂ (20 mg, 16 μL, 0.26 mmol) was added dropwise without separating the excess Mg and MgCl₂. The deep blue solution immediately turned red-brown upon addition of the CS₂. The solution was separated from magnesium by filtration, the solvent was removed *in vacuo* (1×10⁻³ mbar), and the solid residue was dried at 35 °C (water bath) for 30 minutes. The residue was re-dissolved in benzene (4 mL) and the product was crystallized from a minimal amount of fresh benzene at 4 °C. Only a few crystals could be isolated from the viscous solution. A larger amount of the product could not be obtained.

Single crystals suitable for X-ray diffraction can be grown from a saturated benzene solution at 4 °C.

The following analytical data are from the reaction solution since a larger amount of the product could not be isolated. The Raman spectrum was recorded from a single crystal cleaned under the microscope. The IR spectrum was taken from a selected single crystal.

C₁₀₀H₁₀₀Mg₂N₄P₄S₆ (1722.82 g/mol). **Mp.** 203 °C (decomp.). **CHN** calc. (found) in %: C 69.72 (73.87), H 5.85 (6.60), N 3.25 (3.56), S 11.17 (4.67). The deviation of the elemental analysis results from the difficulties of synthesis (light, humidity, air, see section 3.2). **¹H NMR** (25 °C, C₆D₆, 500.1 MHz): δ = *The ¹H NMR spectrum is not evaluable due to the width of the signals and various by-products. The ¹H NMR spectrum is shown in Figure S11.* **³¹P{¹H} NMR** (25 °C, C₆D₆, 121.5 MHz): δ = 73.0 (d, $J(^{31}\text{P}, ^{31}\text{P}) = 26$ Hz), 161.4 (dd, $J(^{31}\text{P}, ^{31}\text{P}) = 10$ Hz, $J(^{31}\text{P}, ^{31}\text{P}) = 16$ Hz), 230.9 (d, $J(^{31}\text{P}, ^{31}\text{P}) = 10$ Hz), 263.5 (s, 2 P, $[P(\mu\text{-N}^{\text{Ter}}\text{Cl})_2]$), 351.7 (s, 1 P, $\text{MgCl}[(\text{TerN})_2\text{P}]\cdot\text{thf}$). **IR** (ATR, 25 °C, 32 Scans, cm⁻¹): $\tilde{\nu}$ = 3361 (m), 2965 (m), 2945 (m), 2914 (m), 2854 (m), 2730 (w), 2118 (w), 2046 (w), 1632 (m), 1611 (m), 1574 (m), 1521 (w), 1482 (m), 1438 (m), 1416 (m), 1374 (m), 1241 (m), 1212 (m), 1140 (m), 1080 (m), 1069 (m), 1030 (s), 913 (m), 884 (m), 847 (vs), 795 (s), 752 (s), 738 (s), 678 (vs), 643 (s), 631 (s), 610 (s), 596 (s), 550 (s), 538 (s), 525 (s), 497 (s), 455 (vs), 433 (vs). **Raman** (633 nm, 10 s, 20 scans, cm⁻¹): $\tilde{\nu}$ = 3062 (5), 3051 (5), 3009 (5), 2947 (5), 2942 (5), 2916 (8), 2856 (5), 2731 (4), 1612 (5), 1580 (5), 1520 (8), 1481 (3), 1437 (3), 1404 (4), 1379 (4), 1304 (9), 1284 (3), 1271 (3), 1246 (2), 1238 (3), 1218 (4), 1201 (3), 1188 (2), 1164 (2), 1117 (2), 1103 (2), 1096 (2), 1087 (3), 1078 (2), 1006 (2), 992 (8), 983 (1), 947 (1), 927 (1), 915 (1), 895 (1), 859 (1), 848 (1), 810 (1), 788 (1), 769 (1), 755 (1), 738 (3), 708 (2), 684 (1), 649 (1), 615 (1), 607 (1), 601 (1), 591 (1), 577 (10), 557 (3), 549 (2), 526 (4), 509 (1), 499 (1), 480 (1), 474 (1), 466 (2), 424 (1), 413 (4), 402 (3), 389 (2), 379 (2), 371 (5), 350 (1), 334 (1), 317 (2), 273 (3), 253 (2), 240 (3), 212 (2).

Figure S11. NMR, IR and Raman spectra of $\{[\text{SP}(\mu\text{-Nter})\text{PS}]\text{TerNCCSMg}\}_2$ (solvent signals indicated by asterisks).

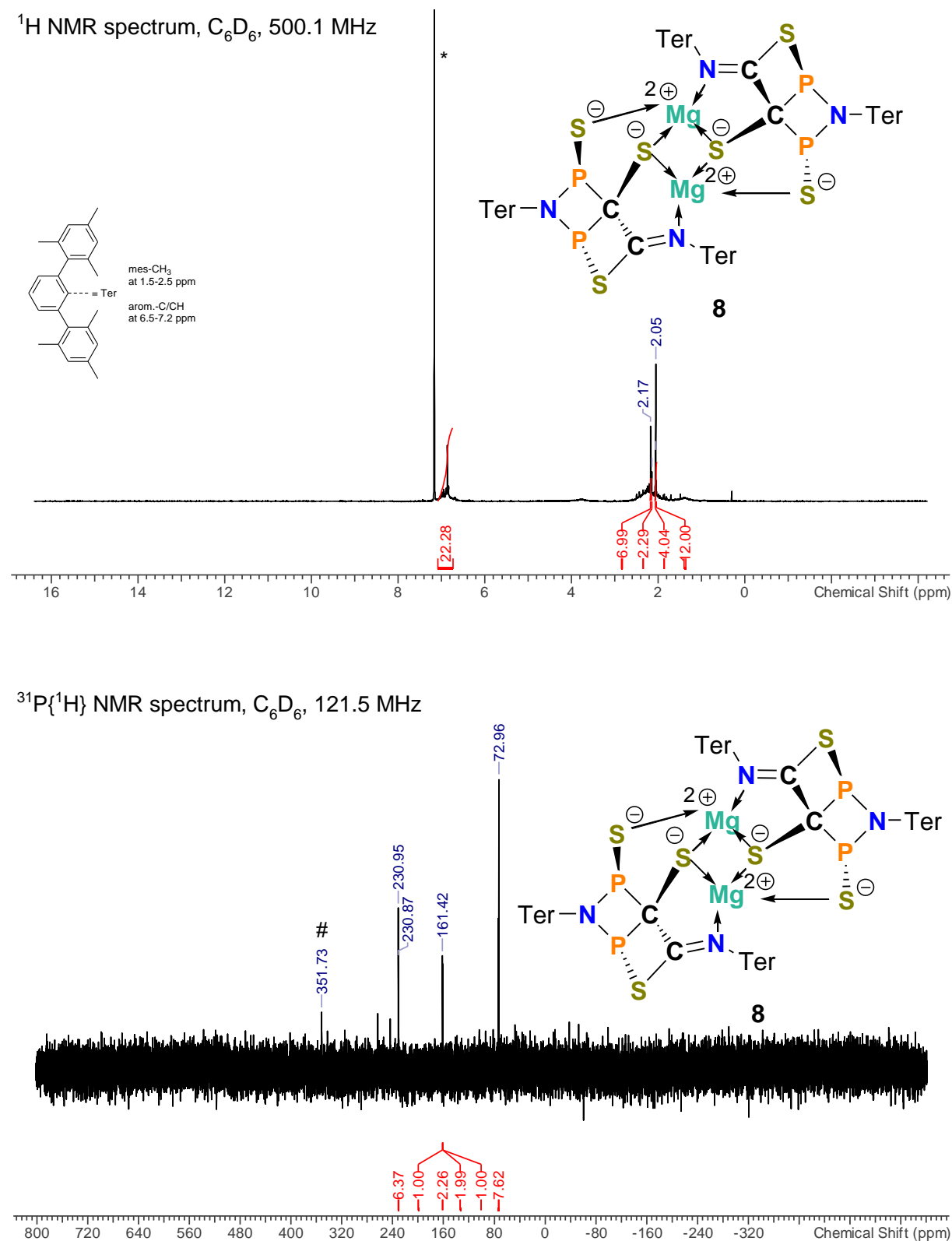
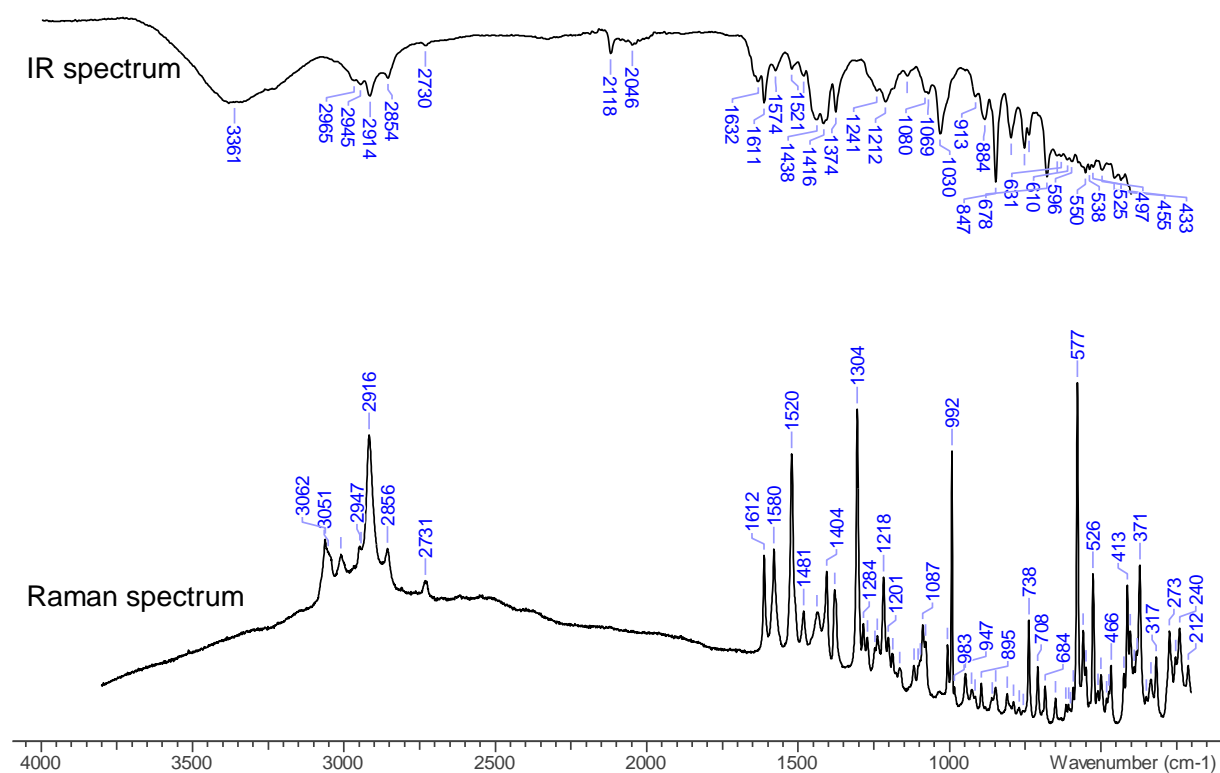
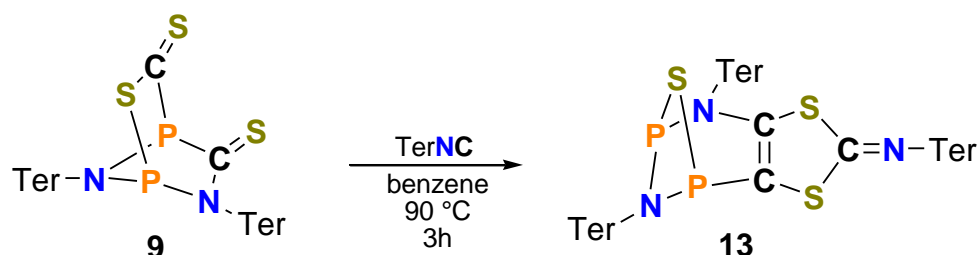


Figure S11. continued.



3.6 Thermal treatment of $[P(\mu\text{-N}^{\text{Ter}})]_2(\text{CS})\cdot\text{CS}_2$ (**9**) – Synthesis of $P_2(\mu\text{-N}^{\text{Ter}})(\mu\text{-S})\text{N}^{\text{Ter}}(\text{CS})_2\text{CN}^{\text{Ter}}$ (**13**)



Note: Compound **9** can only be isolated in 90% purity according to $^{31}\text{P}\{^1\text{H}\}$ NMR spectroscopic data (observed by-products: $[P(\mu\text{-N}^{\text{Ter}})]_2(\text{CSCl}_2)$ (**7**), $[\text{CIP}(\mu\text{-N}^{\text{Ter}})]_2$ and undefinable impurities).

$[P(\mu\text{-N}^{\text{Ter}})]_2(\text{CS})\cdot\text{CS}_2$ (**9**, 20 mg) was dissolved in toluene (5 mL) and the green solution was degassed by several freeze-pump-thaw cycles. The temperature of the solution was then increased stepwise to 90 °C. While stirring for 3 hours at 90 °C the green solution gradually turned yellow. After cooling to ambient temperature all volatile components were removed *in vacuo* (1×10^{-3} mbar) and the yellow residue was dried *in vacuo* (1×10^{-3} mbar) for 30 min at ambient temperature. The residue was re-dissolved in *n*-hexane (10 mL) and the flask was connected with another flask *via* a Schlenk frit. The system was degassed by several freeze-pump-thaw cycles. The insoluble material of the suspension was removed by filtration. After concentration of the filtrate at ambient temperature, the solution was stored at 5 °C overnight, resulting in the deposition of some yellow crystals. Only a few crystals of **13** could be isolated from the viscous solution. Hence, a yield could not be determined.

Single crystals suitable for X-ray diffraction can be grown from saturated *n*-hexane solution at 5 °C.

The Raman spectrum was taken from a single crystal cleaned under the microscope and the melting point was determined using a small single crystal. The NMR spectroscopic data was taken from the reaction solution and not from an isolated product.

C₇₅H₇₅N₃P₂S₃ (1176.59 g/mol). **Mp.** 141 °C (decomp.). **CHN** calc. (found) in %: C 76.56 (54.72), H 6.42 (6.50), N 3.57 (1.44), S 8.18 (1.61). The deviation of the elemental analysis

results from the difficulties of synthesis (light, humidity, air, see section 3.2). **^1H NMR** Due to the large number of different signals and different species, a listing of the data was omitted. The ^1H NMR spectrum is shown in Figure S12. **$^{31}\text{P}\{^1\text{H}\}$ NMR** (25 °C, C_6D_6 , 202.5 MHz): δ = 100.4 (s, $[\text{P}(\mu\text{-N}^-\text{Ter})]_2(\text{CSCl}_2)$ (**7**)), 173.6 (s, $[\text{P}(\mu\text{-N}^-\text{Ter})]_2(\text{CS})\text{CS}_2\text{TerNC}$ (**13**)), 195.2 (s, $[\text{P}(\mu\text{-N}^-\text{Ter})]_2(\text{CSCl}_2)$ (**7**)), 230.6 (s, $[\text{P}(\mu\text{-N}^-\text{Ter})]_2(\text{CS})\text{CS}_2\text{TerNC}$ (**13**)), 263.4 (s, $[\text{PCl}(\mu\text{-N}^-\text{Ter})]_2$), 276.6 (s, $[\text{P}(\mu\text{-N}^-\text{Ter})]_2$ (**1**)), only the signals for the main components are reported. **Raman** (633 nm, 5 s, 5 scans, cm^{-1}): $\tilde{\nu}$ = 3075 (0), 3046 (1), 3007 (1), 2918 (3), 2885 (1), 2871 (1), 2857 (1), 2730 (0), 1646 (0), 1611 (1), 1596 (4), 1576 (6), 1488 (10), 1431 (1), 1429 (1), 1403 (2), 1378 (1), 1301 (3), 1280 (2), 1265 (1), 1247 (1), 1229 (1), 1199 (3), 1191 (1), 1165 (1), 1160 (1), 1094 (1), 1075 (1), 1003 (1), 945 (1), 931 (1), 825 (0), 812 (0), 804 (0), 736 (0), 722 (1), 653 (1), 646 (1), 589 (2), 580 (3), 562 (2), 550 (3), 536 (2), 523 (1), 508 (4), 491 (2), 461 (1), 447 (1), 432 (1), 421 (0), 402 (1), 365 (1), 348 (1), 323 (1), 240 (2), 210 (1), 178 (1), 130 (4), 104 (5), 76 (6).

Figure S12. NMR and Raman spectra of $\text{P}_2(\mu\text{-N}^-\text{Ter})(\mu\text{-S})\text{N}^-\text{Ter}(\text{CS})_2\text{CN}^-\text{Ter}$ (solvent signals indicated by asterisks).

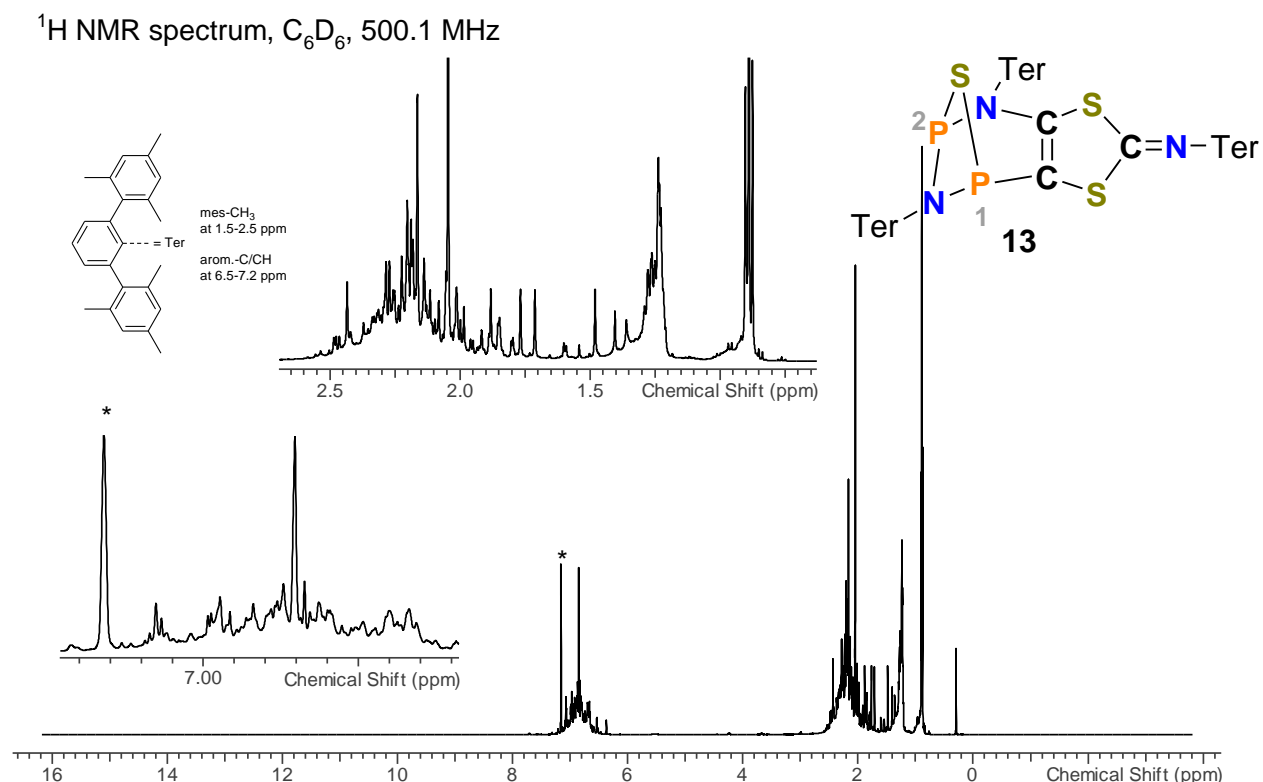
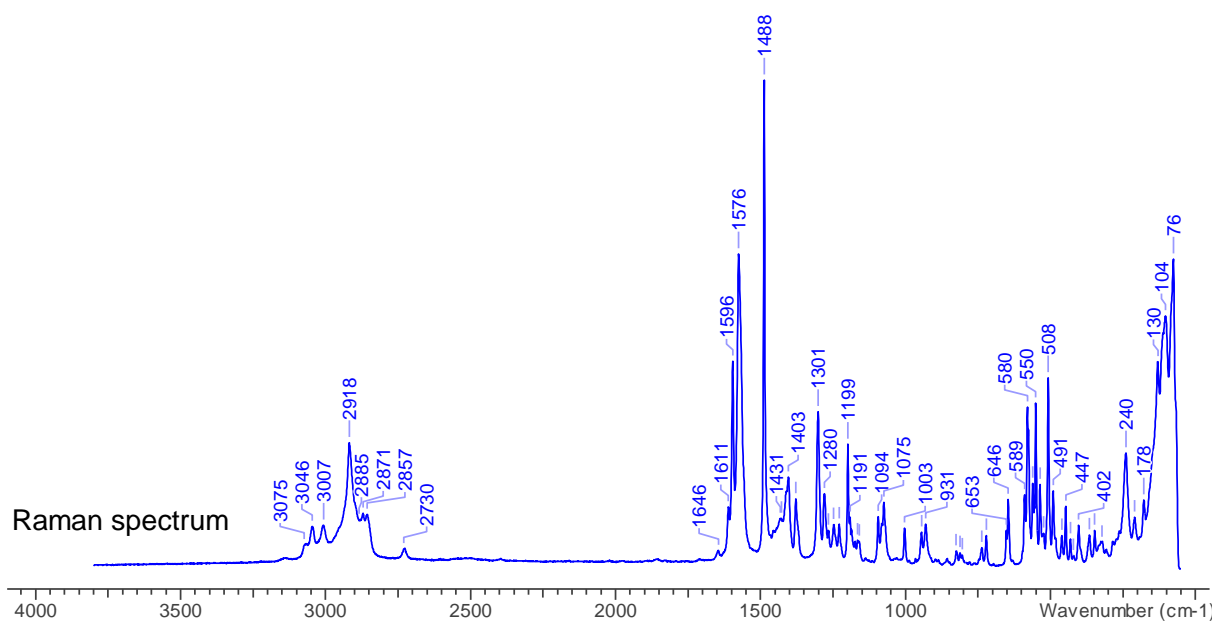
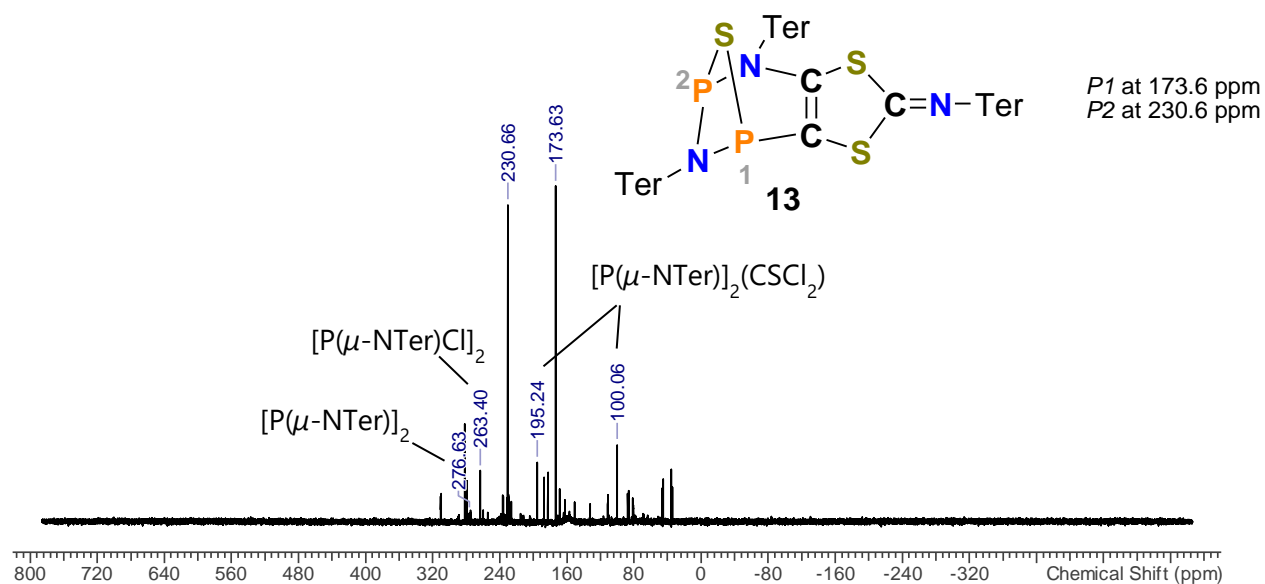
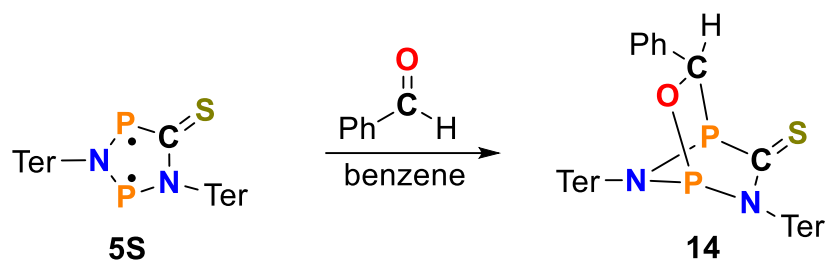


Figure S12. continued.

$^{31}\text{P}\{^1\text{H}\}$ NMR spectrum, C_6D_6 , 202.5 MHz



3.7 $[\text{P}(\mu\text{-N}^{\bullet}\text{Ter})]_2(\text{CS})\cdot\text{PhCHO}$ (**14**)



Note: Due to the very strong light sensitivity of the biradical **5S**, it should be prepared freshly and *in situ*. As soon as the biradical **5S** is irradiated with light decomposition reactions begin. Such a freshly prepared solution of **5S** has a purity of ca. 90% (see chapter 3.2).

All experiments were attempted as best as possible under complete exclusion of light to avoid decomposition of the biradical.

$[\text{P}(\mu\text{-N}^{\bullet}\text{Ter})]_2(\text{CS})$ (200 mg, 0.26 mmol) was dissolved in benzene (10 mL) and benzaldehyde (28 mg, 27 μL , 0.26 mmol) was added dropwise. An immediate colour change from deep blue to yellow was observed. After stirring for 10 minutes at ambient temperature, all volatile components were removed *in vacuo* (1×10^{-3} mbar) and the yellow residue was dried *in vacuo* (1×10^{-3} mbar) for 30 min at 50 °C (water bath). The residue was re-dissolved in *n*-hexane (40 mL) and the flask was connected to another flask via a Schlenk frit. The system was degassed by several freeze-pump-thaw cycles and the suspension was heated up to 60 °C for 15 minutes. The insoluble material of the saturated suspension was removed by filtration. After concentration of the filtrate at 50 °C, the solution was stored at ambient temperature overnight, resulting in the deposition of yellow crystals. The supernatant was removed by syringe and the crystals were dried *in vacuo* (1×10^{-3} mbar) for 30 minutes at 50 °C (water bath). Yield: 60 mg (0.07 mmol, 27%).

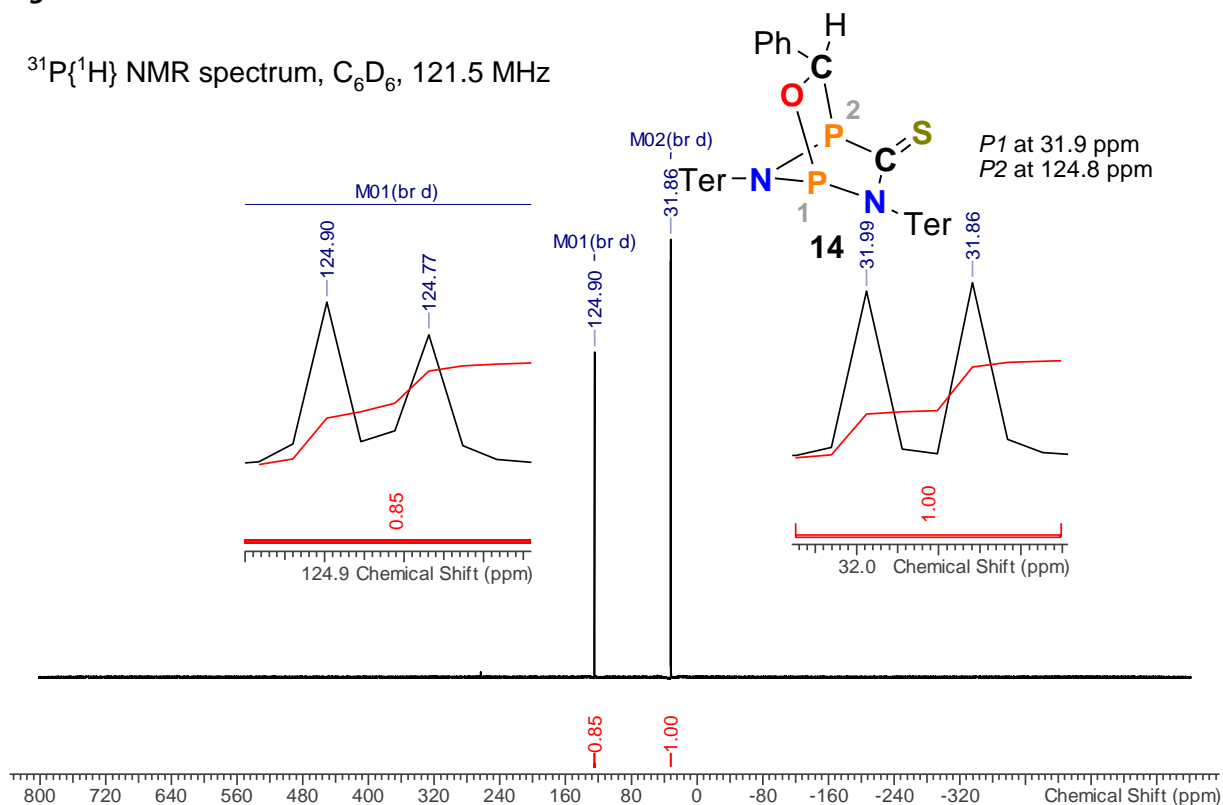
Single crystals suitable for X-ray diffraction can be grown from saturated *n*-hexane solution at ambient temperature.

C₅₆H₅₆N₂OP₂S (867.02 g/mol). **Mp.** 140 °C (decomp.). **CHN** calc. (found) in %: C 77.57 (77.34), H 6.51 (6.53), N 3.23 (3.22), S 3.70 (3.70). **¹H NMR** (25 °C, C₆D₆, 300.1 MHz): δ = 1.00 (s, 6H, CH₃), 1.50 (s, 6H, CH₃), 1.91 (s, 6H, CH₃), 2.01 (s, 6H, CH₃), 2.05 (s, 6H, CH₃), 2.13 (s, 12H, CH₃), 2.17 (s, 6H, CH₃), 2.22 (s, 6H, CH₃), 2.35 (s, 6H, CH₃), 2.41 (s, 6H, CH₃), 2.50 (s, 6H, CH₃), 3.71 (d, 1H, $^2J(^1H, ^{31}P) = 9.1$ Hz, PCH), 3.73 (d, 1H, $^2J(^1H, ^{31}P) = 9.1$ Hz, PCH), 7.00 (m, CH). **¹³C{¹H} NMR** (25 °C, C₆D₆, 125.8 MHz): δ = 14.0 (s, CH₃), 20.1 (s, CH₃), 20.6 (s, CH₃), 20.7 (s, CH₃), 20.7 (s, CH₃), 21.1 (s, CH₃), 21.1 (s, CH₃), 21.1 (s, CH₃), 21.2 (s, CH₃), 21.6 (s, CH₃), 21.8 (s, CH₃), 21.9 (s, CH₃), 21.9 (s, CH₃), 22.0 (s, CH₃), 22.1 (s, CH₃), 22.3 (s, CH₃), 22.5 (s, CH₃), 22.7 (s, CH₂), 31.6 (s, CH₂), 83.9 (d, $^1J(^1H, ^{13}C) = 6$ Hz, PCH), 84.2 (d, $^1J(^1H, ^{13}C) = 6$ Hz, PCH), 123.1 (s, CH), 126.9 (s, CH), 127.1 (s, CH), 127.2 (s, CH), 127.6 (s, CH), 127.8 (s, CH), 128.0 (s, CH), 128.0 (s, CH), 128.2 (s, CH), 128.3 (s, CH), 128.4 (s, CH), 128.5 (s, CH), 128.8 (s, CH), 129.5 (s, CH), 129.8 (s, CH), 130.4 (s, CH), 130.8 (s, CH), 131.2 (s, CH), 131.8 (s, CH), 132.4 (s, CH), 133.5 (s, CH), 135.8 (s, CH), 136.1 (s, CH), 136.3 (s, CH), 136.4 (s, CH), 136.7 (s, CH), 136.7 (s, CH), 136.8 (s, CH), 137.0 (s, CH), 137.0 (s, CH), 137.0 (s, CH), 137.1 (s, CH), 137.3 (s, CH), 137.4 (s, CH), 137.6 (s, CH), 137.9 (s, CH), 137.9 (s, CH), 138.0 (s, CH), 138.0 (s, CH), 138.3 (s, CH), 138.4 (s, CH), 138.7 (s, CH), 138.8 (s, CH), 138.8 (s, CH), 138.8 (s, CH), 139.0 (s, CH), 139.1 (s, CH), 140.8 (s, CH), 141.9 (s, CH). **³¹P{¹H} NMR** (25 °C, C₆D₆, 121.5 MHz): δ = 31.9 (d, 1P, $^2J(^1H, ^{31}P) = 16$ Hz), 124.8 (d, 1P, $^2J(^1H, ^{31}P) = 16$ Hz). **¹⁴N NMR** (25 °C, C₆D₆, 18.1 MHz): No signals observed. **¹⁵N HMBC NMR** (25 °C, C₆D₆, 50.7 MHz): No signals observed. **Raman** (633 nm, 10 s, 10 scans, cm⁻¹): $\tilde{\nu}$ = 3067 (2), 3058 (2), 3051 (2), 3039 (2), 3024 (2), 3017 (2), 2944 (2), 2917 (5), 2883 (2), 2856 (1), 2730 (1), 1611 (5), 1599 (3), 1581 (2), 1495 (1), 1484 (1), 1446 (1), 1435 (1), 1407 (1), 1380 (3), 1374 (2), 1304 (9), 1286 (1), 1271 (1), 1243 (1), 1230 (1), 1211 (3), 1189 (2), 1179 (3), 1164 (1), 1160 (1), 1156 (1), 1094 (3), 1033 (2), 1006 (2), 1001 (10), 988 (1), 966 (1), 947 (1), 928 (1), 913 (1), 886 (1), 859 (1), 850 (1), 793 (1), 788 (1), 763 (1), 750 (1), 740 (2), 699 (1), 664 (1), 652 (3), 619 (1), 594 (1), 578 (10), 560 (4), 552 (4), 544 (2), 523 (3), 517 (1), 511 (1), 501 (1), 493 (1),

Figure S13. NMR, IR and Raman spectra of $[\text{P}(\mu\text{-Nter})]_2(\text{CS})\cdot\text{PhCHO}$ (solvent signals indicated by asterisks).

Figure S13. continued.

$^{31}\text{P}\{^1\text{H}\}$ NMR spectrum, C_6D_6 , 121.5 MHz



$^{13}\text{C}\{^1\text{H}\}$ NMR spectrum, C_6D_6 , 125.8 MHz

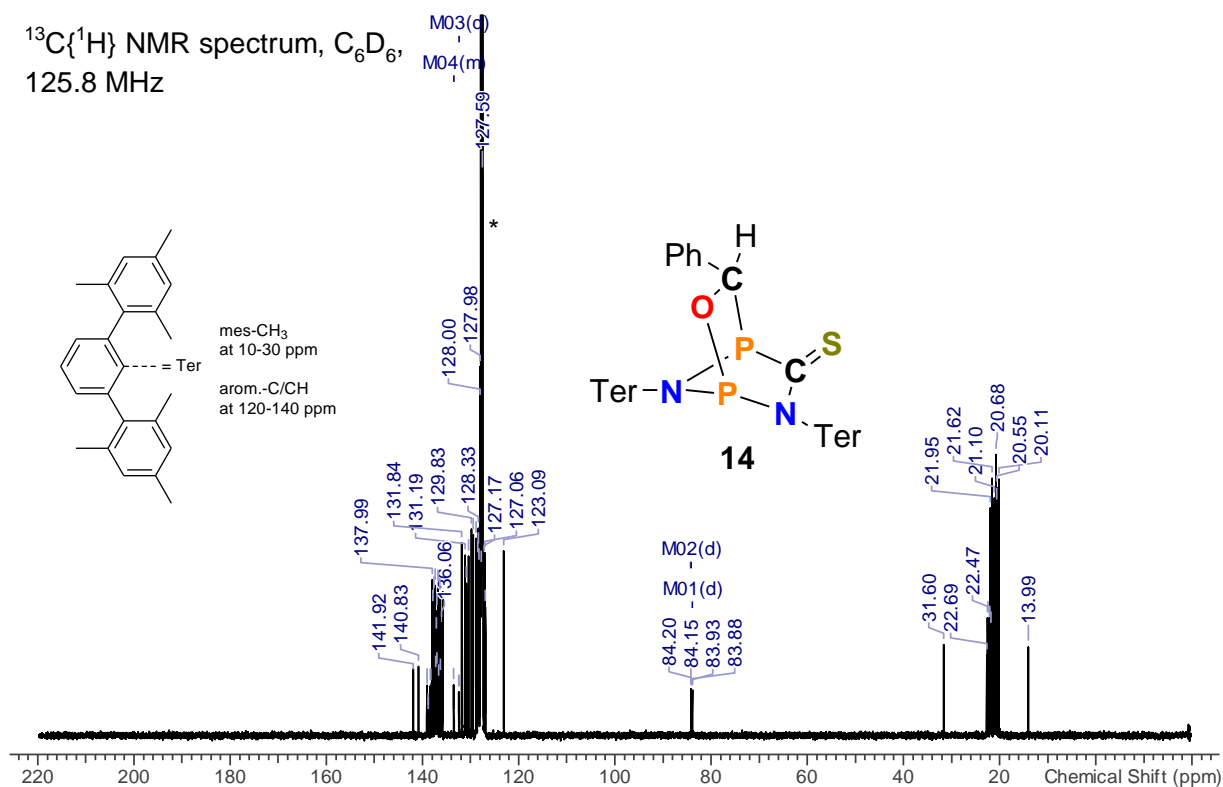
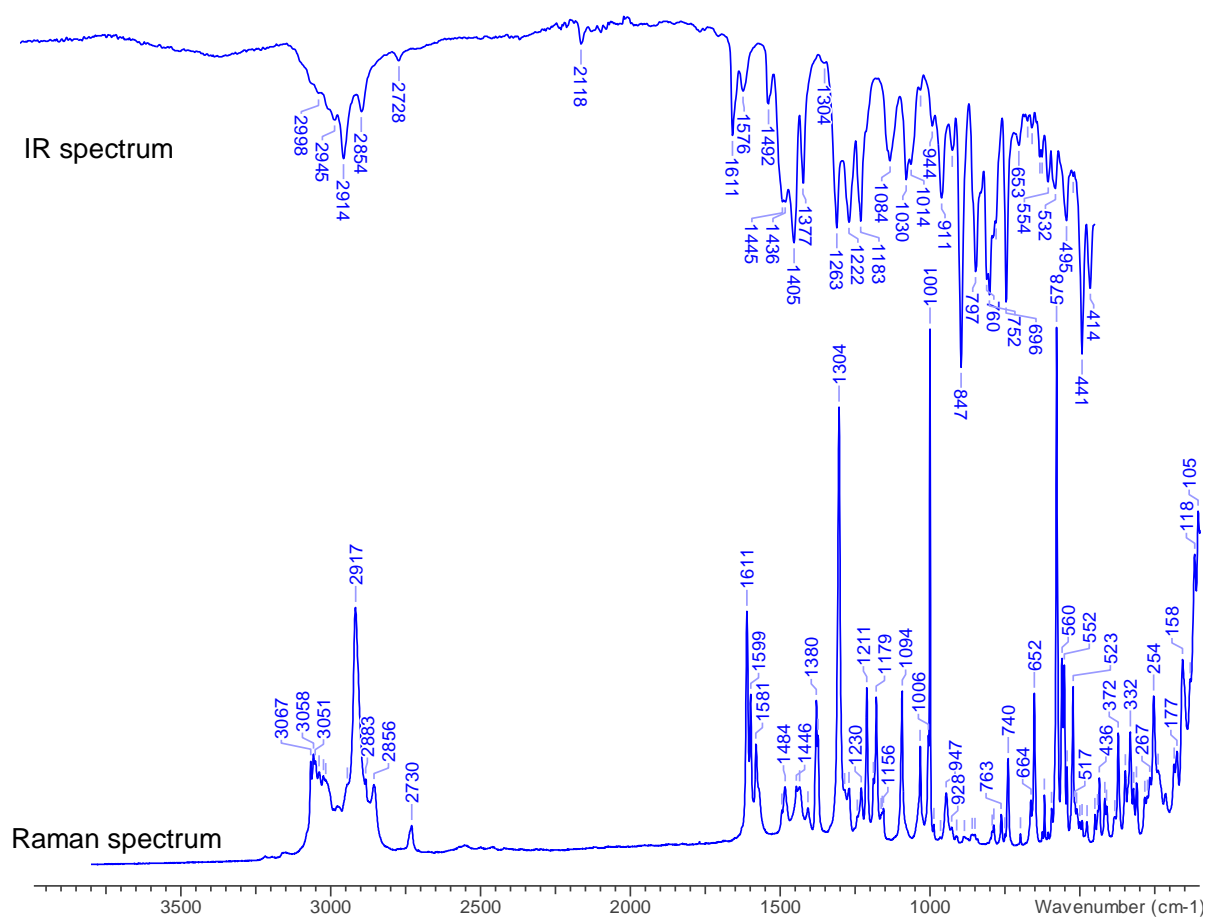


Figure S13. continued.



4 Additional spectroscopic data

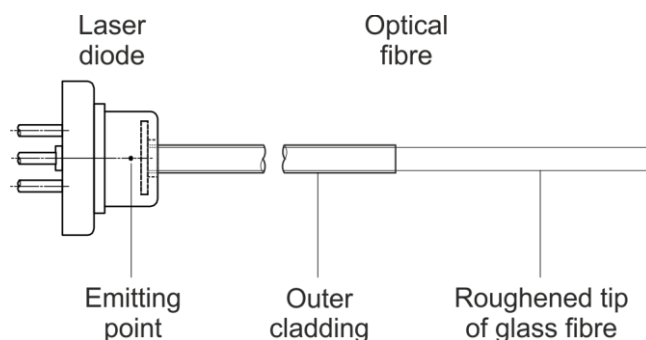
4.1 NMR spectroscopy under irradiation

To facilitate NMR spectroscopy under irradiation, we adopted a setup previously published by the Gschwind group,⁵ who used a fibre-coupled light emitting diode (LED) to direct light into the NMR spectrometer.

In the original publication, the optical fibre was coupled with an LED by placing the polished end of the fibre directly on top of the diode. Unlike commercial solutions, this simple setup does not depend on sophisticated lens systems to focus light into the optical fibre; nonetheless, it offers efficient coupling since the area of the diode is almost completely covered by the cross section of the optical fibre.

Instead of an LED, we decided to use a laser diode (Oclaro HL63193MG, 638 nm, 700 mW), primarily due to the high optical output power at a low price (≈ 80 €) and secondly due to the narrow emission spectrum. Since the opening of the laser diode was only somewhat larger than the cross section of the optical fibre (10 m multimode fibre, 0.39 NA, high OH, 1000 μm core diameter, ThorLabs FT1000UMT), we decided to use the same optical coupling between the diode and the optical fibre as described above (**Figure S14**).

Figure S14. Schematic view of the laser diode and the optical fibre. Efficient coupling was achieved by mounting the fibre directly onto the glass window of the diode



The diode was mounted in a metal casing to dissipate heat. The casing accepts a screw-on brass cylinder that can be used to fix the optical fibre directly on top of the diode and that also serves as an additional heat sink. Moreover, the cylinder may be inserted into an aluminium block ($70 \times 70 \times 30 \text{ mm}^3$) to further dissipate heat (**Figure S15**)

Figure S15. Photo (left) and schematic depiction (right) of the coupling between laser diode and optical fibre (A: laser diode, B: metal casing, C: brass cylinder with a PTFE insert to hold the optical fibre, D: aluminium block, E: optical fibre).

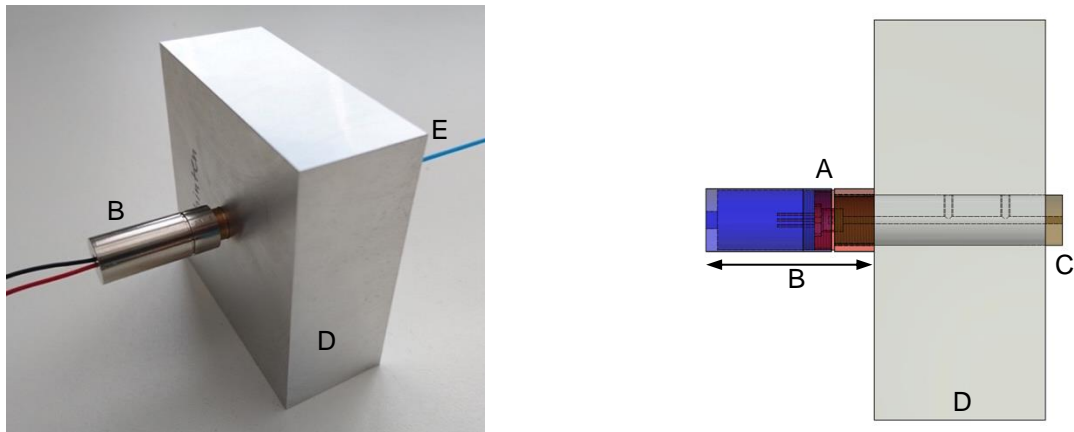
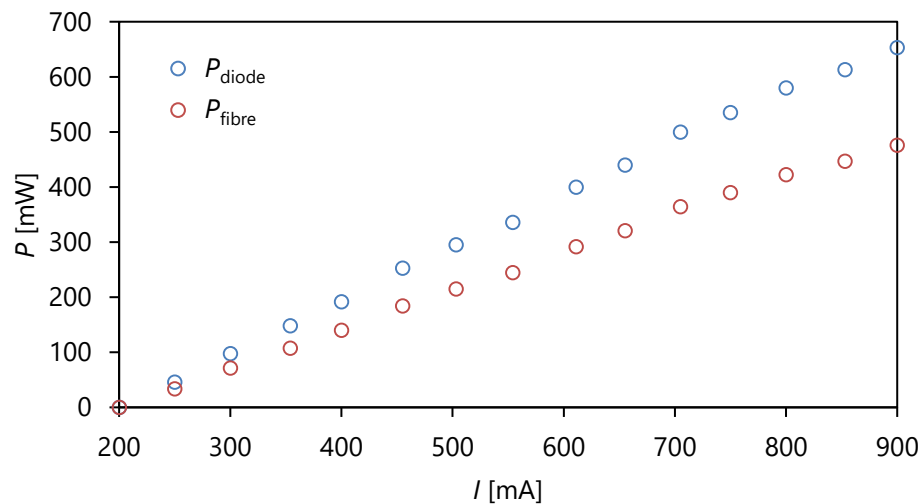


Figure S16. Optical output power measured at the diode (P_{diode}) and at the end of the optical fibre (P_{fibre}).



The optical coupling factor was determined by the ratio of the optical output power at the end of the optical fibre and directly at the diode (neglecting absorption/scattering

within the optical fibre). With a value of 0.73, the coupling is quite efficient. The output power of the optical fibre was measured to be about 480 mW at a maximum current of 900 mA (Figure S16). The diode can run continuously at 500 mA (215 mW optical output) for more than one hour. At currents above 700 mA, heat quickly becomes a problem and the diode can only be switched on for short intervals of time.

As described in the original publication of the Gschwind group,⁵ the outer cladding of the optical fibre was removed at the tip and the glass surface was roughened to allow uniform irradiation of the sample within the spectrometer. The fibre was inserted into an NMR tube with a coaxial insert (Figure S17). To ensure inert conditions, all samples were prepared in a glovebox and the tubes were sealed with custom-made PTFE caps as well as 2–3 layers of PTFE tape.

Figure S17. Schematic view of an NMR tube with coaxial insert and optical fibre.

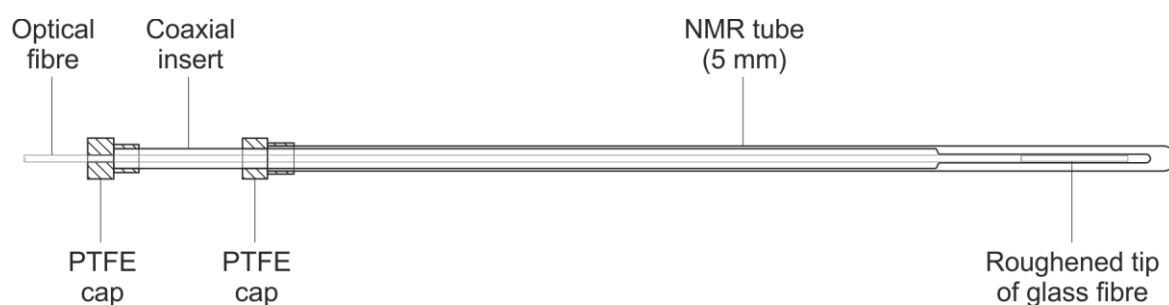
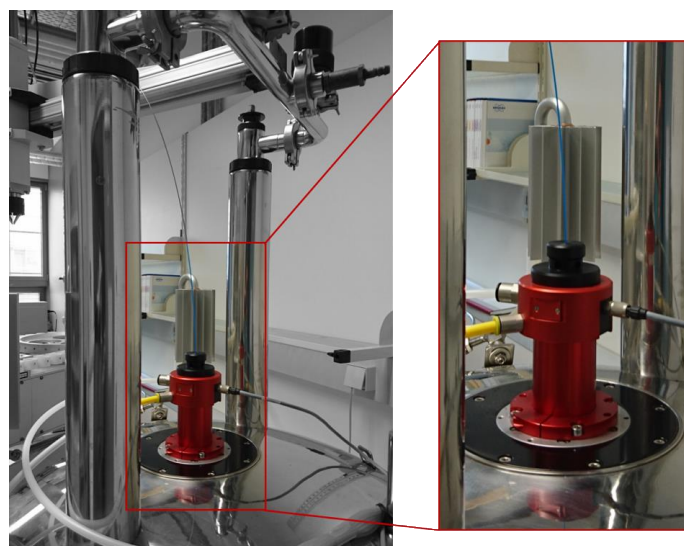


Figure S18. The sample inlet is equipped with a cap which ensures that the optical fibre is centred above the NMR tube.



To ensure that the optical fibre cannot exert lateral forces and thereby tilt the NMR tube in the spectrometer, a cap with a central bore was placed on top of the spectrometer's sample inlet. The optical fibre is passed through the bore to keep it centred above the NMR tube (**Figure S18**).

4.2 Photoisomerization of compound 5S

Figure S19. $^{31}\text{P}\{^1\text{H}\}$ NMR spectra of **5S** in the dark (bottom) and **6S** under irradiation with red light (top).

$^{31}\text{P}\{^1\text{H}\}$ spectra at -20 °C

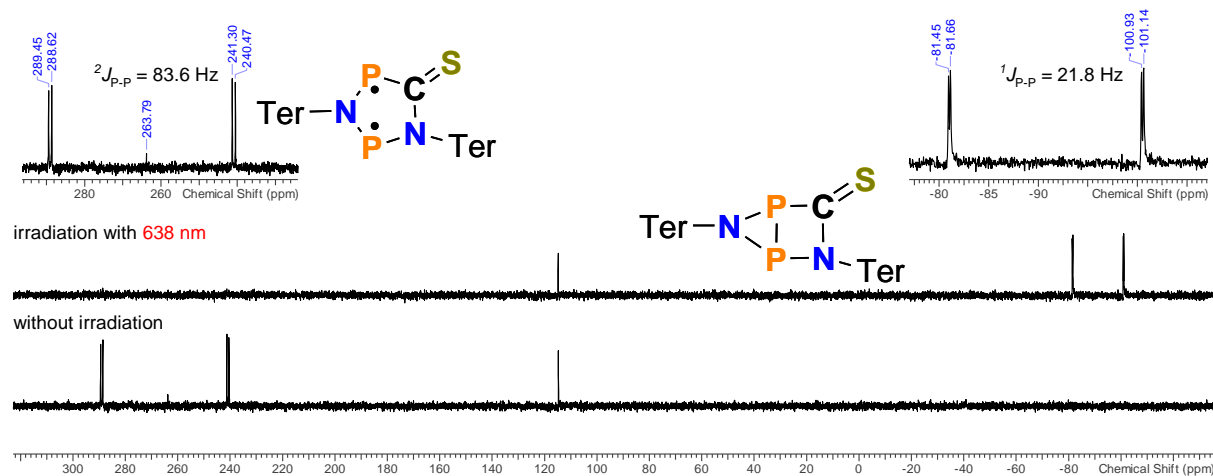


Figure S20. Time-resolved $^{31}\text{P}\{^1\text{H}\}$ NMR spectra of **6S** recorded after irradiation (bottom).

$^{31}\text{P}\{^1\text{H}\}$ NMR spectra at ambient temperature

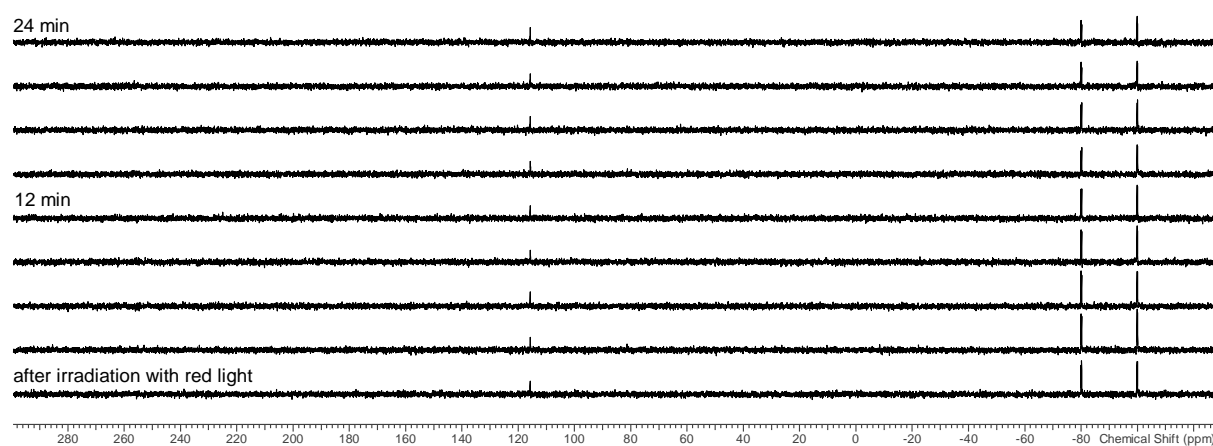


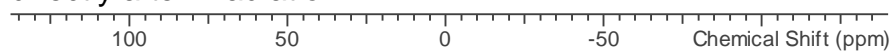
Figure S21. $^{31}\text{P}\{^1\text{H}\}$ NMR spectra of **6S**. Decomposition was observed.

$^{31}\text{P}\{^1\text{H}\}$ NMR spectra

2h after irradiation



directly after irradiation



4.3 $^{31}\text{P}\{^1\text{H}\}$ NMR data

The following tables contain experimental $^{31}\text{P}\{^1\text{H}\}$ NMR spectroscopic data. Calculated values are given in brackets for comparison (GIAO method, PBE0-D3/def2-TZVP).

Table S3. $^{31}\text{P}\{^1\text{H}\}$ NMR spectroscopic data of different isomers of compound 7.

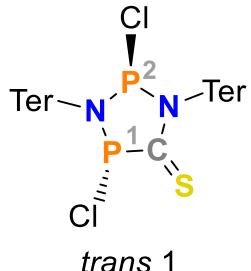
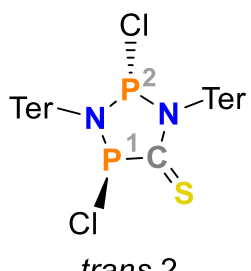
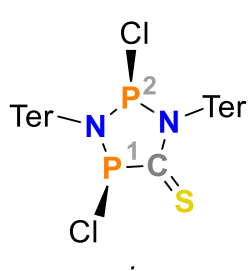
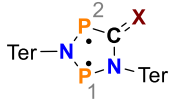
isomer	δ [ppm]	
	<i>P1</i>	<i>P2</i>
 <i>trans 1</i>	98.3 (+113.5)	175.2 (+218.0)
 <i>trans 2</i>	100.2 (+125.1)	195.4 (+196.6)
 <i>cis</i>	96.6 (107.1)	162.2 (205.2)

Table S4. Selected ^{31}P NMR spectroscopic and UV-Vis data for comparison.

species	5S		5O ⁶		5NDmp ⁷	
 <p>5O $\text{X} = \text{O}$ 5S $\text{X} = \text{S}$ 5Dmp $\text{X} = \text{NDmp}$</p>	<i>P1</i>	<i>P2</i>	<i>P1</i>	<i>P2</i>	<i>P1</i>	<i>P2</i>
$\delta_{\text{exp.}} / \text{ppm}$	242.7	289.1	197.4	254.1	221.5	258.1
$^2J_{\text{exp.}}(^{31}\text{P}, ^{31}\text{P}) / \text{Hz}$	88		94		135	
$\lambda_{\text{max.}} / \text{nm}$	638		531		643	

5 Computational details

5.1 General remarks

Computations were carried out using Gaussian09⁸ or ORCA 4.2.1.⁹

Structure optimizations employed the pure DFT exchange-correlation functional PBE^{10,11} in conjunction with Grimme's dispersion correction D3(BJ)^{12,13} and the def2-TZVP basis set¹⁴ (notation PBE-D3/def2-TZVP). The resolution of identity (RI) approximation was employed, using Weigend's accurate Coulomb fitting basis.¹⁵ All structures were fully optimized and confirmed as minima by frequency analyses.

More accurate electronic energies for optimized structures were computed by single-point DLPNO-CCSD(T)^{16–19} calculations employing the def2-TZVP basis set¹⁴ and def2-TZVP/C correlation fitting basis²⁰ (notation: DLPNO-CCSD(T)/def2-TZVP//PBE-D3/def2-TZVP). Thermodynamic quantities at this level of theory were calculated using the DLPNO-CCSD(T) single point energy and the thermal corrections at the PBE-D3/def2-TZVP level of theory. The T_1 diagnostic was evaluated to ensure reliable results (empirically, CCSD(T) results are considered reliable if $T_1 < 0.02$).²¹

Ab-initio calculations using multiconfigurational wavefunctions were performed using ORCA 4.2.1. The Complete Active Space SCF (CASSCF) method was employed,^{22–29} which correctly describes the multireference character of the investigated systems (i.e. treatment of non-dynamic correlation).

5.2 Summary of calculated data

5.2.1 Thermodynamic data

Table S5. Summary of calculated data, including electronic energies and thermal corrections.

Compd.	PG	Opt. method	$E_{\text{tot}}^{[a]}$	$\Delta G^{[b]}$	$E_{\text{CCSD(T)}}^{[c]}$	T_1
5S biradical	C ₁	PBE-D3/ def2-TZVP	−3085.6254	0.7346	−3082.6292	0.011
6S housane	C ₁		−3082.6120	0.7358	−3082.6123	0.011
7 trans1	C ₁		−4005.7527	0.7352	−4002.1473	0.011
7 trans2	C ₁		−4002.7503	0.7336	−4002.1447	0.011
7 cis	C ₁		−4002.7432	0.7351	−4002.1364	0.011

[a] Total SCF energy in a.u.; [b] thermal correction to Gibbs energy in a.u. (298 K); [c] single-point DLPNO-CCSD(T)/def2-TZVP energy.

5.2.2 Isomerisation energies

Table S6. Isomerisation energies (DLPNO-CCSD(T)/def2-TZVP//PBE-D3/def2-TZVP, in kJ·mol^{−1}).

Reaction	ΔE^{tot}	$\Delta_R H$	$\Delta_R G^\circ$
5S → 6S	+44.4	+44.7	+47.5
7 trans1 → 7 trans2	+7.0	+6.3	+2.8
7 trans 1 → 7 cis	+28.6	+28.1	+28.4

5.3 Biradical character

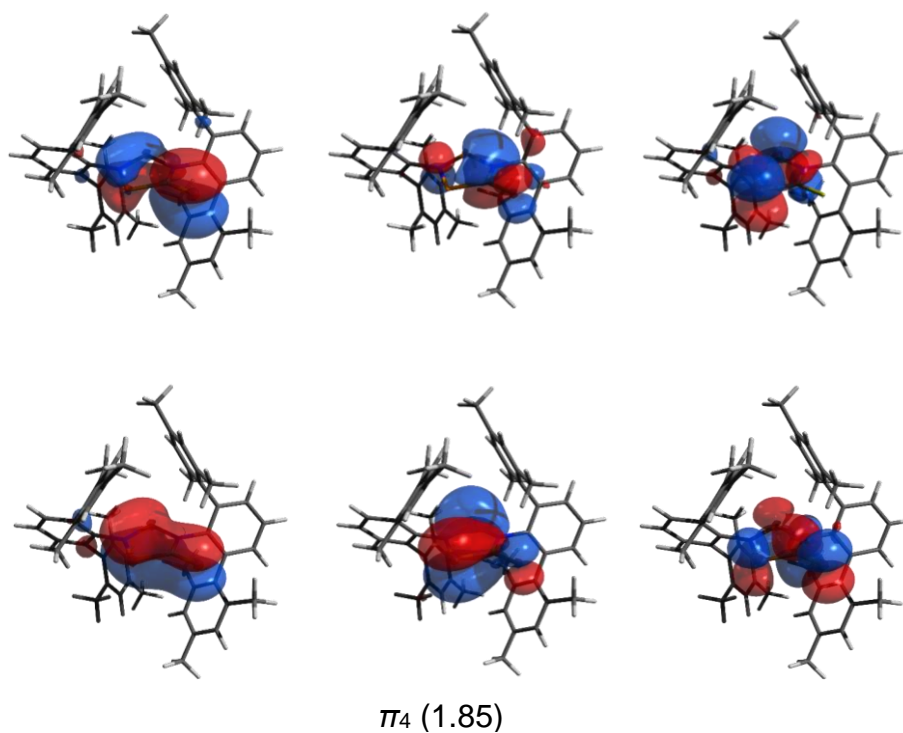
The multiconfigurational wavefunction of **5S** was computed at the CASSCF(8,6)/def2-TZVP level of theory, using the optimized structure at the PBE-D3/def2-TZVP level of theory (see above). All π -type orbitals were included in the active space. The biradical character was estimated using the β scale suggested by Xantheas et al.³⁰

$$\beta = \frac{2c_2^2}{c_1^2 + c_2^2}$$

Table S7. CAS-Cl expansion coefficients of the most important contributions to the wave function ($|c_i| > 0.1$).

#	configuration	c_i^2
1	222200	0.898
2	222020	0.064

Figure S22. Graphical representations of the active orbitals of **5S**. The orbital occupation numbers of the CAS calculation are given.



6 References

- 1 J. Bresien, T. Kröger-Badge, S. Lochbrunner, D. Michalik, H. Müller, A. Schulz and E. Zander, A chemical reaction controlled by light-activated molecular switches based on hetero-cyclopentanediyIs, *Chem. Sci.*, 2019, **10**, 3486–3493.
- 2 G. M. Sheldrick, SHELXT – Integrated space-group and crystal-structure determination, *Acta Crystallogr. Sect. A Found. Adv.*, 2015, **71**, 3–8.
- 3 G. M. Sheldrick, Crystal structure refinement with SHELXL, *Acta Crystallogr. Sect. C Struct. Chem.*, 2015, **71**, 3–8.
- 4 G. M. Sheldrick, SADABS Version 2, 2004, Univ. Göttingen, Ger.
- 5 C. Feldmeier, H. Bartling, E. Riedle and R. M. Gschwind, LED based NMR illumination device for mechanistic studies on photochemical reactions – Versatile and simple, yet surprisingly powerful, *J. Magn. Reson.*, 2013, **232**, 39–44.
- 6 A. Hinz, A. Schulz and A. Villinger, Stable Heterocyclopentane-1,3-diyIs, *Angew. Chem. Int. Ed.*, 2015, **54**, 2776–2779.
- 7 A. Hinz, A. Schulz and A. Villinger, Tunable Cyclopentane-1,3-diyIs Generated by Insertion of Isonitriles into Diphosphadiazanediyls, *J. Am. Chem. Soc.*, 2015, **137**, 9953–9962.
- 8 M. J. Frisch, G. W. Trucks, H. B. Schlegel, G. E. Scuseria, M. A. Robb, J. R. Cheeseman, G. Scalmani, V. Barone, B. Mennucci, G. A. Peterson, H. Nakatsuji, M. Caricato, X. Li, H. P. Hratchian, A. F. Izmaylov, J. Bloino, G. Zheng, J. L. Sonnenberg, M. Hada, M. Ehara, K. Toyota, R. Fukuda, J. Hasegawa, M. Ishida, T. Nakajima, Y. Honda, O. Kitao, H. Nakai, T. Vreven, J. A. Montgomery Jr., J. E. Peralta, F. Ogliaro, M. Bearpark, J. J. Heyd, E. Brothers, K. N. Kudin, V. N. Staroverov, T. Keith, R. Kobayashi, J. Normand, K. Raghavachari, A. Rendell, J. C. Burant, S. S. Iyengar, J. Tomasi, M. Cossi, N. Rega, J. M. Millam, M. Klene, J. E. Know, J. B. Cross, V. Bakken, C. Adamo, J. Jaramillo, R. Gomperts, R. E. Stratmann, O. Yazyev, A. J. Austin, R. Cammi, C. Pomelli, J. W. Ochterski, R. L. Martin, K. Morokuma, V. G. Zakrzewski, G. A. Voth, P. Salvador, J. J. Dannenberg, S. Dapprich, A. D. Daniels, O. Farkas, J. B. Foresman, J. V. Ortiz, J. Cioslowski and D. J. Fox, Gaussian 09, Revision E.01, 2013, Inc., Wallingford CT.
- 9 F. Neese, Software update: the ORCA program system, version 4.0, *Wiley Interdiscip. Rev. Comput. Mol. Sci.*, 2018, **8**, 1327.
- 10 J. P. Perdew, K. Burke and M. Ernzerhof, Generalized Gradient Approximation Made Simple, *Phys. Rev. Lett.*, 1996, **77**, 3865–3868.
- 11 J. P. Perdew, K. Burke and M. Ernzerhof, Generalized Gradient Approximation Made Simple, *Phys. Rev. Lett.*, 1997, **78**, 1396–1396.
- 12 S. Grimme, J. Antony, S. Ehrlich and H. Krieg, A consistent and accurate ab initio parametrization of density functional dispersion correction (DFT-D) for the 94

- elements H-Pu, *J. Chem. Phys.*, 2010, **132**, 154104.
- 13 S. Grimme, S. Ehrlich and L. Goerigk, Effect of the damping function in dispersion corrected density functional theory, *J. Comput. Chem.*, 2011, **32**, 1456–1465.
 - 14 F. Weigend and R. Ahlrichs, Balanced basis sets of split valence, triple zeta valence and quadruple zeta valence quality for H to Rn: Design and assessment of accuracy., *Phys. Chem. Chem. Phys.*, 2005, **7**, 3297–305.
 - 15 F. Weigend, Accurate Coulomb-fitting basis sets for H to Rn, *Phys. Chem. Chem. Phys.*, 2006, **8**, 1057–1065.
 - 16 C. Riplinger and F. Neese, An efficient and near linear scaling pair natural orbital based local coupled cluster method, *J. Chem. Phys.*, 2013, **138**, 34106.
 - 17 D. G. Liakos, M. Sparta, M. K. Kesharwani, J. M. L. Martin and F. Neese, Exploring the Accuracy Limits of Local Pair Natural Orbital Coupled-Cluster Theory, *J. Chem. Theory Comput.*, 2015, **11**, 1525–1539.
 - 18 C. Riplinger, P. Pinski, U. Becker, E. F. Valeev and F. Neese, Sparse maps-A systematic infrastructure for reduced-scaling electronic structure methods. II. Linear scaling domain based pair natural orbital coupled cluster theory, *J. Chem. Phys.*, 2016, **144**, 024109.
 - 19 D. G. Liakos, Y. Guo and F. Neese, Comprehensive Benchmark Results for the Domain Based Local Pair Natural Orbital Coupled Cluster Method (DLPNO-CCSD (T)) for Closed- and Open-Shell Systems, *J. Phys. Chem. A*, 2020, **124**, 90–100.
 - 20 A. Hellweg, C. Hättig, S. Höfener and W. Klopper, Optimized accurate auxiliary basis sets for RI-MP2 and RI-CC2 calculations for the atoms Rb to Rn, *Theor. Chem. Acc.*, 2007, **117**, 587–597.
 - 21 C. J. Cramer, *Essentials of Computational Chemistry: Theories and Models*, *Essentials of Computational Chemistry: Theories and Models*, , John Wiley & Sons, Ltd, Chichester, UK, 2004.
 - 22 D. Hegarty and M. A. Robb, Application of unitary group methods to configuration interaction calculations, *Mol. Phys.*, 1979, **38**, 1795–1812.
 - 23 R. H. A. Eade and M. A. Robb, Direct minimization in mc scf theory. the quasi-newton method, *Chem. Phys. Lett.*, 1981, **83**, 362–368.
 - 24 H. B. Schlegel and M. A. Robb, MC SCF gradient optimization of the $\text{H}_2\text{CO} \rightarrow \text{H}_2 + \text{CO}$ transition structure, *Chem. Phys. Lett.*, 1982, **93**, 43–46.
 - 25 F. Bernardi, A. Bottoni, J. J. W. McDouall, M. A. Robb and H. B. Schlegel, MCSCF gradient calculation of transition structures in organic reactions, *Faraday Symp. Chem. Soc.*, 1984, **19**, 137.
 - 26 P. E. M. Siegbahn, A new direct CI method for large CI expansions in a small orbital space, *Chem. Phys. Lett.*, 1984, **109**, 417–423.
 - 27 M. Frisch, I. N. Ragazos, M. A. Robb and H. Bernhard Schlegel, An evaluation of three direct MC-SCF procedures, *Chem. Phys. Lett.*, 1992, **189**, 524–528.

- 28 N. Yamamoto, T. Vreven, M. A. Robb, M. J. Frisch and H. Bernhard Schlegel, A direct derivative MC-SCF procedure, *Chem. Phys. Lett.*, 1996, **250**, 373–378.
- 29 M. Klene, M. A. Robb, M. J. Frisch and P. Celani, Parallel implementation of the CI-vector evaluation in full CI/CAS-SCF, *J. Chem. Phys.*, 2000, **113**, 5653–5665.
- 30 E. Miliordos, K. Ruedenberg and S. S. Xantheas, Unusual Inorganic Biradicals: A Theoretical Analysis, *Angew. Chemie Int. Ed.*, 2013, **52**, 5736–5739.